

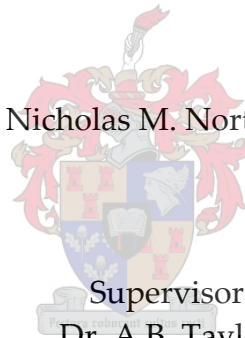
# THE MODELLING AND CONTROL OF AN AUTOMOTIVE DRIVETRAIN

Thesis presented in partial fulfilment of the requirements for the degree

**MASTER OF SCIENCE IN ENGINEERING**

By

Nicholas M. Northcote



Supervisor

Dr. A.B. Taylor

Department of Mechanical Engineering  
University of Stellenbosch

Co-Supervisor

Mr. J. Treurnicht

Department of Electrical and Electronic Engineering  
University of Stellenbosch

April 2006

## Declaration

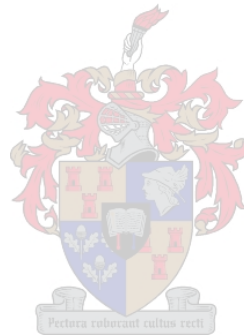
I, the undersigned, declare that the work contained in this thesis is my own original work and has not previously, in its entirety or in part, been submitted at any university for a degree.

---

Signature of Candidate

---

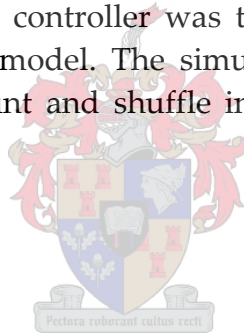
Date



## Abstract

Shunt and shuffle in a vehicle drivetrain are two driveability related phenomena responsible for driver discomfort. They are experienced as a sharp jerk (shunt) followed by a series of longitudinal oscillations (shuffle) and are induced by a rapid change in engine torque. The use of drive-by-wire throttles in modern day vehicles enables the onboard electronic control unit to manipulate the driver's torque demand before sending a revised torque demand signal to the engine. In this way a feedback control system can be used to ensure that the drivetrain follows the driver's torque demand as quickly as possible without inducing shunt or shuffle.

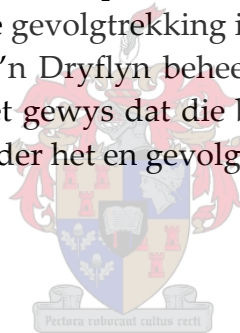
In this project a drivetrain model was derived and its parameters experimentally determined. The accuracy of the model was validated using test data from a vehicle, and the conclusion was made that the model was an accurate vehicle simulation tool. A drivetrain controller was then designed and its performance simulated using the vehicle model. The simulations showed that the controller significantly reduced the shunt and shuffle in the drivetrain thereby improving driver comfort.



## Samevatting

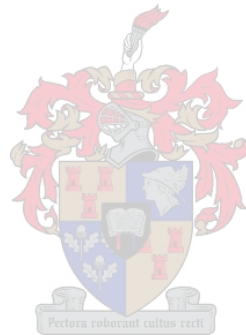
'Shunt' en 'shuffle' in 'n voertuig is 'n oorsaak van bestuurdersongemak. Hierdie verskynsels word ondervind as 'n skerp rukbeweging ('shunt') gevolg deur 'n reeks horisontale oorgangsverskynsels ('shuffle'), en gebeur as gevolg van 'n skielike verandering in enjindraaimoment. Die gebruik van 'drive-by-wire' smoorleppe in moderne voertuie maak dit moontlik vir die motor se elektroniese beheereenheid om die bestuurder se draaimomentvereiste te wysig. 'n Hersiende draaimoment aanvraag kan dan na die enjin gestuur word. 'n Terugvoer-beheerstelsel kan dus gebruik word om te verseker dat die dryflyn die draaimomentvereiste van die bestuurder so vinnig as moontlik sal volg, sonder om 'shunt' of 'shuffle' te veroorsaak.

In hierdie projek is 'n dryflyn model afgelei en sy eksperimentele parameters bepaal. Data afkomstig van toetse op 'n voertuig is gebruik om die akuraatheid van die model te bevestig. Die gevolgtrekking is gemaak dat die model 'n akkurate voertuig simulasiemiddel is. 'n Dryflyn beheerder is ontwerp en die prestasie is gesimuleer. Die simulaties het gewys dat die beheerder die 'shunt' en 'shuffle' in die dryflyn aansienlik verminder het en gevolglik is bestuurdersgemak verbeter.



## Acknowledgements

First of all I would like to thank my supervisor Dr. Andrew Taylor for teaching me to search for reasons why dreams can be achieved rather than for reasons why they can't. Thank you also to my co-supervisor Mr. Johan Treurnicht for all his patience and guidance over the last year. A special mention of thanks goes to Cobus and Ferdi Zietsman for all their help with the experimental work in this thesis. Finally on a more personal note, I am deeply grateful to my parents George and Brunella. Thank you for your never ending love and support, and for teaching me the basic principles of honesty and hard work.



# Contents

Declaration	i
Abstract	ii
Samevatting	iii
Acknowledgements	iv
Contents	v
List of Figures	viii
List of Tables	x
Glossary	xi
Chapter 1: Introduction	1
1.1 Project Background	1
1.2 Project Objectives	3
1.3 Project Outline	3
1.4 Chapter Overview	4
Chapter 2: Literature Review	5
2.1 Introduction	5
2.2 Vehicle Driveability	5
2.3 Drivetrain Modelling	6
2.4 Drivetrain Control	8
Chapter 3: Drivetrain Modelling	11
3.1 Introduction	11
3.2 Complex Model	12
3.2.1 Engine, Flywheel and Clutch	12
3.2.2 Transmission and Driveshaft	13
3.2.3 Wheel and Vehicle	14
3.2.4 Summary	16
3.3 Simplified Model	16
Chapter 4: Parameter Identification	20
4.1 Introduction	20
4.2 Experimental Apparatus	20
4.2.1 Test-Rig	20
4.2.2 Sensors	22



4.2.2.1	Torque	22
4.2.2.2	Speed	23
4.3	Data Acquisition	24
4.3.1	Analogue Signals	24
4.3.2	Digital Signals	24
4.4	Experimental Procedures	25
4.4.1	Inertia	25
4.4.2	Friction	26
4.4.3	Stiffness	27
4.4.4	Damping	28
4.5	Results	28
4.5.1	D.C. Motor	29
4.5.2	Engine	30
4.5.3	Flywheel	31
4.5.4	Clutch	31
4.5.5	Transmission	31
4.5.6	Driveshaft	32
4.5.7	Wheel and Brake-Disk	32
4.5.8	Vehicle	32
Chapter 5: System Simulation		33
5.1	Introduction	33
5.2	Working Points	33
5.3	Simulations	34
5.3.1	Complex vs. Simplified Model	34
5.3.2	Effect of Gear Ratio	36
5.4	Verification of Simulation Accuracy	37
5.4.1	Published Results	37
5.4.2	Vehicle Measurements	37
Chapter 6: Controller Development		40
6.1	Introduction	40
6.2	Control Strategy	40
6.3	Estimator Design	42
6.3.1	Estimator Theory	42



---

6.3.2 Drivetrain Estimator	43
6.3.3 Estimator Gains	44
6.3.4 Estimator Performance	45
6.4 Control System	48
Chapter 7: Controller Performance	49
7.1 Introduction	49
7.2 Control Gains	49
7.3 Controller Performance Analysis	52
7.4 Comparison with Torque Rate Limiter	56
7.5 Possible Improvements	57
Chapter 8: Conclusion	58
References	60
Appendix A: Drivetrain Model	A.1
Appendix B: Test-Rig	B.1
Appendix C: Drivetrain Parameters	C.1
Appendix D: Discrete Estimator	D.1





## List of Figures

- Figure 1.1.1: Vehicle Response to a Rapid Change in Torque (Johansson (2004))
- Figure 1.1.2: A Volkswagen Jetta
- Figure 1.3.1: Flowchart of the Project Outline
- Figure 2.3.1: Complex vs. Linear Model for a Torque Ramp from 10 Nm to 110 Nm  
(Karlsson, 2001)
- Figure 2.3.2: Complex vs. Linear Model for a Torque Ramp from -20 Nm to 80 Nm  
(Karlsson, 2001)
- Figure 2.4.1: PID Control (Lagerberg and Egardt, 2002)
- Figure 2.4.2: PID Control with Torque Compensator (Lagerberg and Egardt, 2002)
- Figure 2.4.3: Simple Switching Control (Lagerberg and Egardt, 2002)
- Figure 2.4.4: Modified Switching Control (Lagerberg and Egardt, 2002)
- Figure 3.1.1: Drivetrain Inertias
- Figure 3.2.1: Clutch Stiffness Coefficient (Pettersson, 1996)
- Figure 3.2.2: Driveshaft with Backlash
- Figure 3.2.3: Longitudinal Forces on a Vehicle
- Figure 3.2.4: Complex Model Block Diagram
- Figure 3.3.1: Simplified Linear Drivetrain Model
- Figure 3.3.2: Block Diagram of the Simplified Model Transfer Functions
- Figure 4.2.1: Experimental Setup
- Figure 4.2.2: Fully Assembled Test-Rig
- Figure 4.2.3: The Load Cell Setup
- Figure 4.2.4: Digital Magnetic Pick-up Speed Measurement
- Figure 4.4.1: Inertia Test Data
- Figure 4.4.2: Friction Test Data
- Figure 4.4.3: Stiffness Experiment
- Figure 4.4.4: Stiffness Test Data (Maree, 2005)
- Figure 4.5.1: DC Motor Closed-Loop Bandwidth for Different Speed Amplitudes  
(After Conradie, 2001)
- Figure 4.5.2: Engine Torque Model Response
- Figure 5.3.1: Complex vs. Simplified Model (10 Nm to 90 Nm Torque Ramp)
- Figure 5.3.2: Complex vs. Simplified Model (-10 Nm to 70 Nm Torque Ramp)

- Figure 5.3.3: Vehicle Acceleration Response in Different Gears
- Figure 5.4.1: Raw Accelerometer Test Data
- Figure 5.4.2: ECU Estimated Engine Torque Data
- Figure 5.4.3: Measured vs. Modelled Response (-40 Nm to 130 Nm in 0.15 seconds)
- Figure 6.2.1: Control Strategy
- Figure 6.3.1: Engine Speed Measurement Data Noise
- Figure 6.3.2: Estimated vs. Actual (Complex Model) Engine Speed (No Backlash)
- Figure 6.3.3: Estimated vs. Actual (Complex Model) Wheel Speed (No Backlash)
- Figure 6.3.4: Estimated vs. Actual (Complex Model) Engine Speed (Backlash)
- Figure 6.3.5: Estimated vs. Actual (Complex Model) Wheel Speed (Backlash)
- Figure 6.3.6: Modelled Engine Speed with Noise vs. Estimated Engine Speed
- Figure 6.4.1: Schematic Overview of the Control System
- Figure 7.2.1: Controlled Acceleration Response (No Backlash)
- Figure 7.2.2: Response Error vs. Control Gain (No Backlash)
- Figure 7.2.3: Controlled Acceleration Response (Backlash)
- Figure 7.2.4: Response Error vs. Control Gain (Backlash)
- Figure 7.3.1: Uncontrolled vs. Controlled Response (No Backlash)
- Figure 7.3.2: Uncontrolled vs. Controlled Response (Backlash)
- Figure 7.3.3: Uncontrolled vs. Controlled Engine Speed
- Figure 7.3.4: Driver Demand vs. Controlled Engine Torque Demand
- Figure 7.4.1: Torque Rate Limiter vs. Controller (No Backlash)
- Figure 7.4.2: Torque Rate Limiter vs. Controller (Backlash)

## List of Tables

Table 4.1.1: Experimental Procedures

Table 4.5.1: DC Motor Parameters

Table 4.5.2: Clutch Parameters

Table 4.5.3: Transmission Parameters



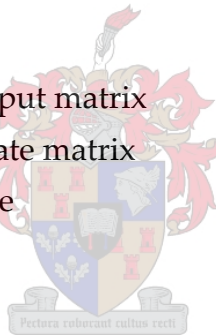
# Glossary

## Nomenclature

DAQ	Data Acquisition
DC	Direct Current
ECU	Electronic Control Unit
IPC	Integrated Powertrain Control
PID	Proportional Integral Derivative
RMS	Root Mean Squared
VSD	Variable Speed Drive

## Symbols

$\Gamma$	Discrete state-space input matrix
$\Phi$	Discrete state-space state matrix
$\alpha$	Half the backlash angle
$\beta$	Road gradient
$\zeta$	Damping ratio
$\theta$	Angular displacement (rad)
$\rho$	Air density
$\omega_n$	Natural frequency
$A$	Vehicle maximum frontal area
$b$	Viscous friction coefficient
$c$	Damping
$c_w$	Vehicle coefficient of drag
$F_a$	Air drag force
$F_g$	Gradient force
$F_r$	Rolling resistance force
$F_t$	Tractive wheel force
$g$	Gravitational acceleration
$i$	Gear Ratio



$I$	Inertia (kg.m <sup>2</sup> )
$k$	Stiffness
$K$	Control Gain
$L$	Estimator gain matrix
$L_{eng}$	Engine transport delay (lag)
$m$	Vehicle mass
$R_v$	Process noise covariance
$R_w$	Measurement noise covariance
$r_w$	Wheel outer radius
$T$	Torque (Nm)
$t_{eng}$	Engine time constant
$u$	System input
$v$	Vehicle velocity
$x$	System state
$y$	System output

## Subscripts

$c$	Clutch
$cc$	Clutch damping
$ck$	Clutch stiffness
$c1$	Clutch from 0 to 12°
$c2$	Clutch from 12° to 14°
$d$	Driveshaft
$f$	Flywheel
$L$	Load
$s$	Driveshaft
$t$	Transmission
$w$	Wheel
$dz$	Dead zone



# Introduction

---

# 1

## 1.1 Project Background

With recent advances in automotive electronics it has become possible to electronically control a vehicle's driveability. The term drivability refers to the driver's perception of the vehicle's response to a certain input. It encompasses a range of aspects including driver comfort, vehicle responsiveness and handling.

Driver comfort has become a major area of research in the automotive industry. Shunt and shuffle in a vehicle drivetrain are two driveability related phenomena responsible for driver discomfort. They are experienced as a sharp jerk (shunt) followed by a series of longitudinal oscillations (shuffle) and are induced by a rapid change in engine torque. The shunt and shuffle phenomena are clearly visible in the vehicle's acceleration response in Figure 1.1.1 (Johansson, 2004). In this thesis, driver comfort is defined as a measure of the amplitude of the shunt and shuffle.

The use of drive-by-wire throttles in modern day vehicles enables the onboard electronic control unit (ECU) to manipulate the driver's torque demand before sending a revised torque demand signal to the engine. In this way controllers can use the engine as a torque actuator to the drivetrain. Drivetrain controllers do exist in modern vehicles, but many of them are simply slew-rate limiters which filter any sharp change in driver torque demand into a slower, smoother signal. Although these systems do prevent shunt and shuffle they are often over-damped, and this results in a vehicle that seems sluggish and slow. This reduction in vehicle responsiveness is unacceptable, and the primary aim of this project was to develop an electronic control system that would reduce the shunt and shuffle without

reducing the vehicle's responsiveness to a torque demand. More specifically, the vehicle's responsiveness is defined as the time taken for the vehicle to reach steady-state acceleration in response to a driver torque demand.

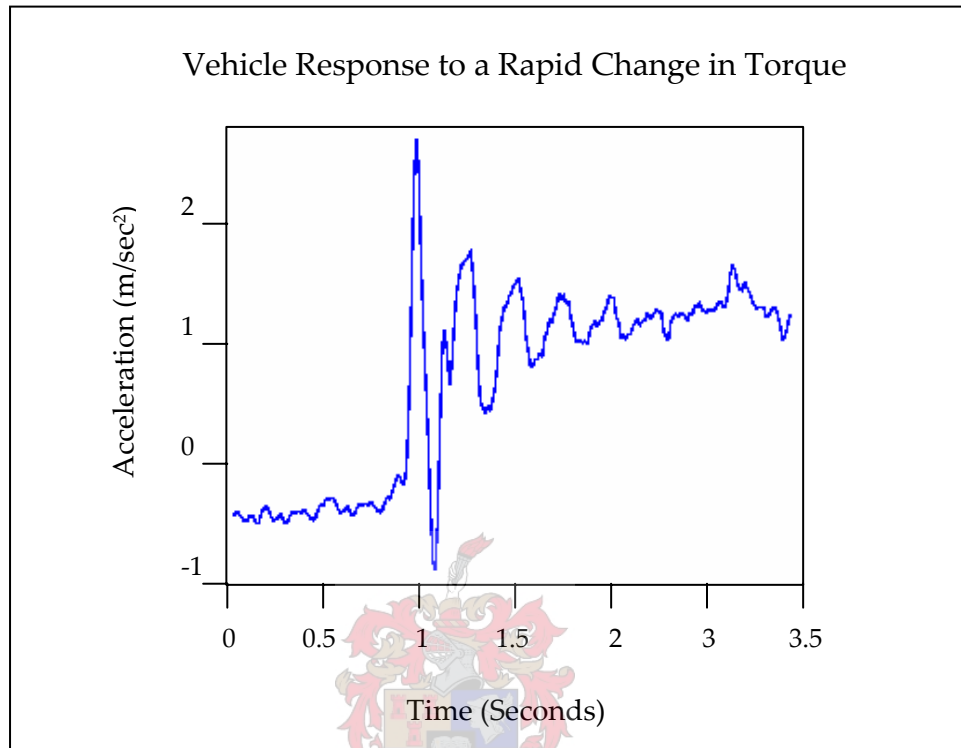


Figure 1.1.1: Vehicle Response to a Rapid Change in Torque (Johansson (2004))

In order to develop a controller, an accurate drivetrain model is required to predict the vehicle's response to a torque input. This model can then be used to design and simulate the control system performance. In this project, the model created was based on a 1.6 litre Volkswagen Jetta (Figure 1.1.2).



Figure 1.1.2: A Volkswagen Jetta

## 1.2 Project Objectives

The primary objectives of this thesis are as follows:

1. The development of an accurate working model for the simulation of the vehicle's longitudinal response to various torque inputs.
2. The design and simulation of a drivetrain controller that will improve driver comfort without reducing vehicle responsiveness.

## 1.3 Project Outline

Figure 1.3.1 is a flow chart of the various steps completed in the project.

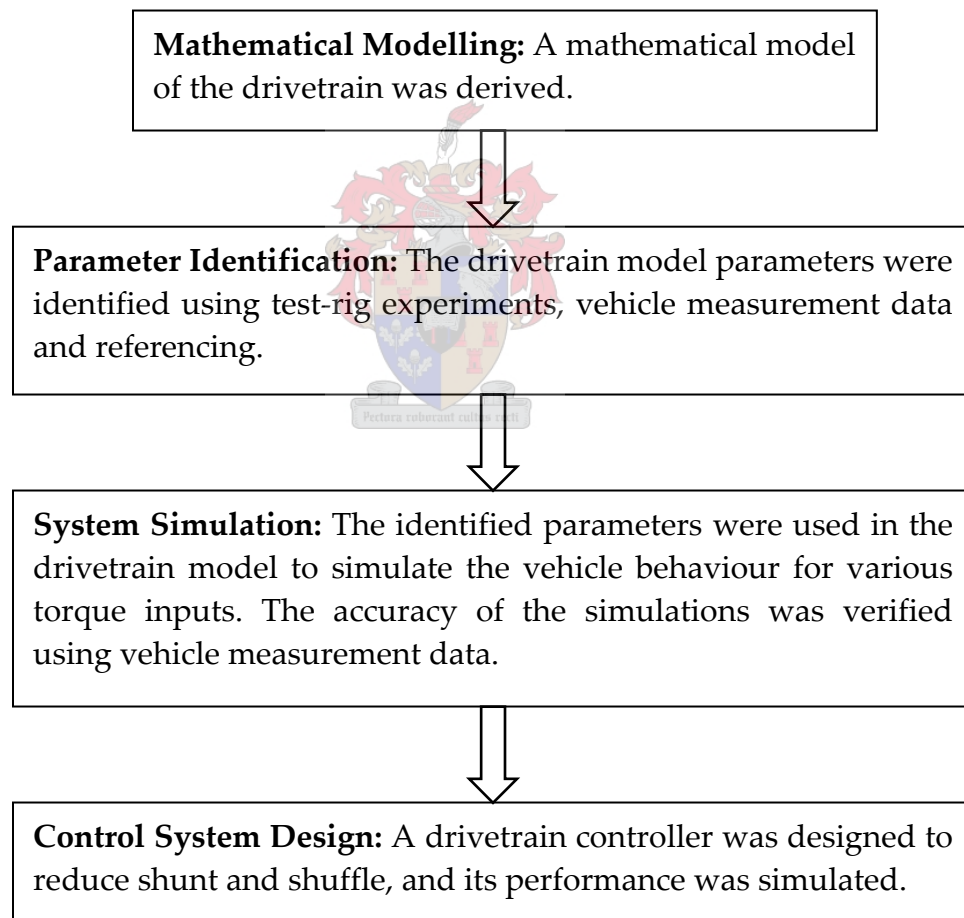


Figure 1.3.1: Flowchart of the Project Outline



## 1.4 Chapter Overview

The project is documented in the following chapters:

### **Chapter 2: Literature Study**

Chapter 2 is a comprehensive literature study describing the automotive drivetrain modelling and control research that has been completed over the last few years.

### **Chapter 3: Drivetrain Modelling**

Two different drivetrain models are derived: A complex non-linear model for accurate simulations, and a simplified third-order model for use in control system development.

### **Chapter 4: Parameter Identification**

This chapter describes the various experimental procedures followed in order to obtain values for the drivetrain model parameters. The results of these procedures are then summarized.

### **Chapter 5: Vehicle Simulation**

The models derived in Chapter 3 are used to simulate the vehicle response to various inputs and conditions. The performance of the complex non-linear model is compared to that of the linear third-order model and the accuracy of the simulations is verified through further experimentation.

### **Chapter 6: Controller Development**

A control strategy and state estimator are derived. The estimator performance is then evaluated in more detail.

### **Chapter 7: Controller Performance**

The performance of the drivetrain controller is analyzed in detail.

### **Chapter 8: Conclusion**

In this chapter, the work completed is summarized and several recommendations are made for possible future work on this topic.

# Literature Review

---

# 2

## 2.1 Introduction

This chapter is a literature review of various publications on the subject of automotive drivetrain modelling and control. The literature study was divided into 3 sections and is summarized in the following paragraphs:

2.2 Vehicle Driveability

2.3 Drivetrain Modelling

2.4 Drivetrain Control

Although much work has been done on the modelling of automotive drivetrains, the development of control systems for improved driveability is a relatively new field.

## 2.2 Vehicle Driveability

Persson (2004) is a literature survey of approximately 80 papers related to various driveability aspects. The study included topics such as customer demands with regards to driveability, the measurement of driveability, the various types of automotive drivetrains, and different approaches taken towards improving vehicle driveability. Persson defined driveability as the term which describes the driver's complex subjective perception of the interactions between driver and vehicle. Various subjective driveability indexes were examined and the need for an objective, standardized way of rating driveability was identified. Persson also investigated various drivetrain models and concluded that simplified drivetrain models are cost-effective tools for developing drivetrain controllers. Different drivetrain controller strategies were briefly examined, and it was concluded that it

is in fact possible to reduce drivetrain oscillations by using an electronic control system.

Johansson (2004) developed a grading system for shunt and shuffle based on an objective mathematical analysis. This work followed the research of Persson (2004) where the need for such a system was identified. The grading system was based on separate tests for shunt and shuffle and an overall grade (mark) was calculated as the average between the shunt grade and the shuffle grade. The mathematical grading system correlated well with the grades assigned by several experienced professional test drivers.

## 2.3 Drivetrain Modeling

Pettersson (1996) derived and validated a drivetrain model for a large truck. He presented three models of increasing complexity and then validated them through experimental testing. The first model presented was a linear model which assumed a stiff clutch, a stiff propeller shaft and viscous friction in the transmission and final drive (differential). The second model added the clutch flexibility to the original linear model. Finally, a more complete non-linear model was derived which included a clutch model with a static non-linearity. The accuracy of each of these models was verified through vehicle measurements and their performances were compared. The following conclusions were made:

1. The main contribution to driveline dynamics from driving torque to engine speed and wheel speed is the driveshaft.
2. Including clutch dynamics in the model doesn't improve the model's accuracy for drivetrain oscillation frequencies below 6 Hz.

Karlsson (2001) presented two drivetrain models of a Volvo passenger car; a linear third-order model and complex non-linear model. The linear model excluded clutch dynamics and backlash. The complex model accounted for both these non-linearities. Karlsson compared the performance of these models for various torque inputs. A similar approach was taken in the current study.

Figure 2.3.1 shows Karlsson's comparison of the complex and linear models for a torque input ramp from 10 Nm to 110 Nm in 0.1 seconds. In this scenario the backlash region is completely avoided and the linear model performs relatively well.

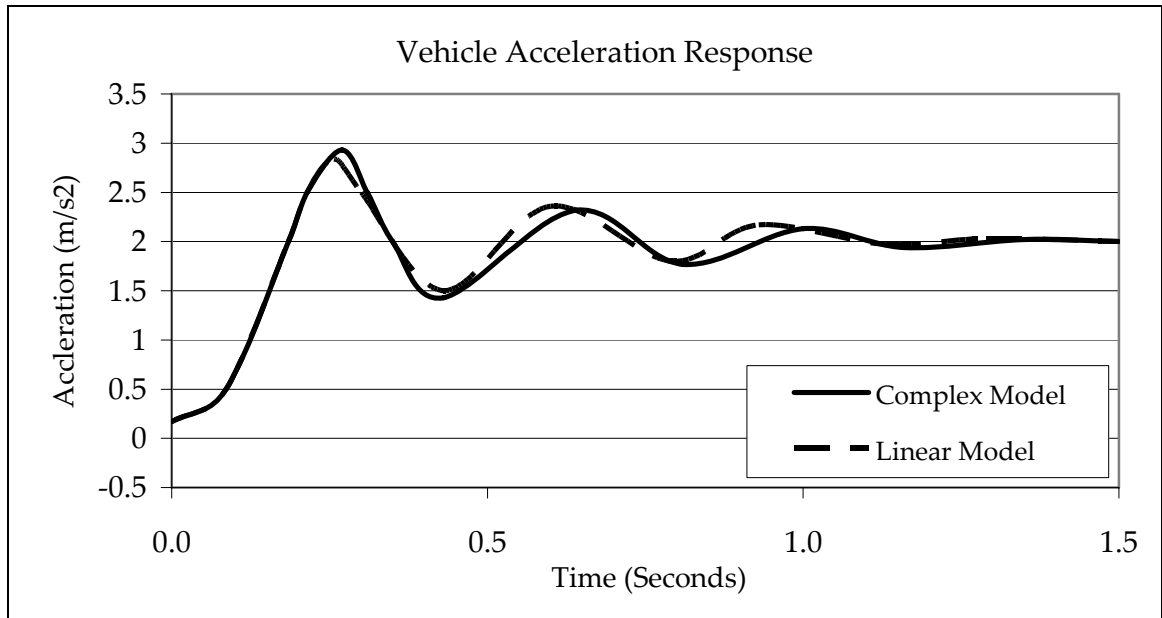


Figure 2.3.1: Complex vs. Linear Model for a Torque Ramp from 10 Nm to 110 Nm (After Karlsson, 2001)

Figure 2.3.2 shows the acceleration responses of Karlsson's complex and linear models for a torque ramp from -20 Nm to 80 Nm in 0.15 seconds. In this scenario the drivetrain passes through the backlash region and the linear model becomes more inaccurate.

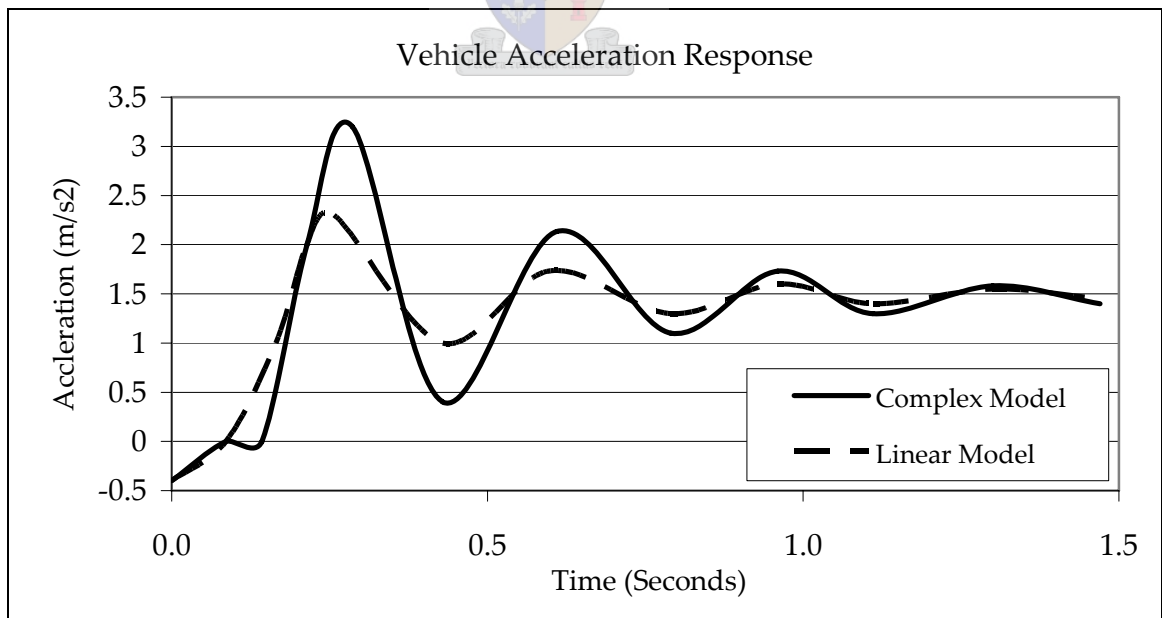


Figure 2.3.2: Complex vs. Linear Model for a Torque Ramp from -20 Nm to 80 Nm (After Karlsson, 2001)

## 2.4 Drivetrain Control

The literature covering drivetrain control is far less extensive than for drivetrain modelling. Most of the research done in this field has been part of the Integrated Powertrain Control (IPC) project between the Chalmers University of Technology in Sweden, and the Volvo Corporation. Shunt and shuffle in an automotive drivetrain are predominantly due to the backlash in the drivetrain as well as the elasticity of various drivetrain components. Karlsson (2001) defines backlash as the small amount of mechanical slack between adjacent movable components.

There are two major approaches that can be used when designing a drivetrain controller to prevent shunt and shuffle. The first is to attempt to actively control the drivetrain as it passes through the backlash region. This strategy requires two control modes; one for when the drivetrain is in the backlash region and another for when it is not. A non-linear backlash model is included in this type of controller. The second approach is a linear approach which doesn't include a backlash model in the controller and simply treats the backlash as a disturbance. This type of controller is designed to be robust enough to handle the disturbance.

Lagerberg (2001) is a literature study covering the modelling and control of backlash in automotive driveshafts. Three strategies are proposed to control the drivetrain; a linear passive controller, a non-linear passive controller and a non-linear active controller. With the linear passive approach, a linear controller was designed that was robust enough to handle the backlash non-linearity without including a model of it in the controller. The non-linear passive strategy included a backlash model, but adopted a careful approach in the backlash region. The non-linear active approach included a backlash model and adopted the philosophy of getting out of backlash region as quickly as possible. Although these strategies were identified, they were not used in simulations.

Lagerberg and Egardt (2002) proposed the following controllers; a standard proportional, integral, differential (PID) controller, a PID controller with a torque compensator, a simple active switching controller and a modified switching controller. The standard PID controller used the load acceleration as the controlled variable. The PID controller with the torque observer used a first-order shaft torque estimate combined with the load acceleration as the control signal. The simple active switching controller switched between two control signals; one when the drivetrain was in the backlash region and another when it was not. This controller excluded the engine dynamics and shaft flexibility. The modified

switching controller had a strategy similar to that of the simple active switching controller, but included the engine dynamics in the backlash mode.

The drivetrain response to a torque step for each of the four controllers is shown in Figures 2.4.1 through to 2.4.4. It is clear that the performance of the different controllers becomes progressively better. Lagerberg and Egardt (2002) conclude that although the switching controllers clearly out-perform the linear PID controllers, if the backlash angle is overestimated these switched controllers become unstable. The switching controllers are therefore not robust enough to implement in an actual vehicle.

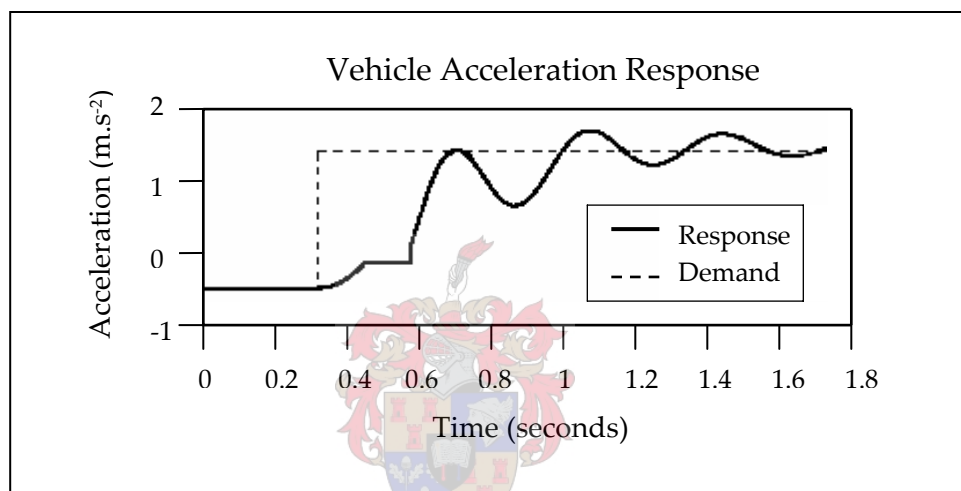


Figure 2.4.1: PID Control (Lagerberg and Egardt, 2002)

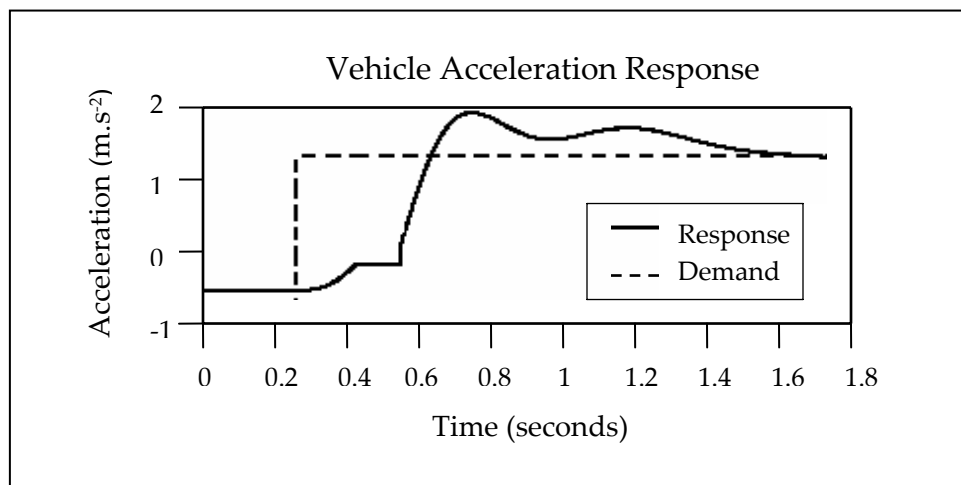


Figure 2.4.2: PID Control with Torque Compensator (Lagerberg and Egardt, 2002)

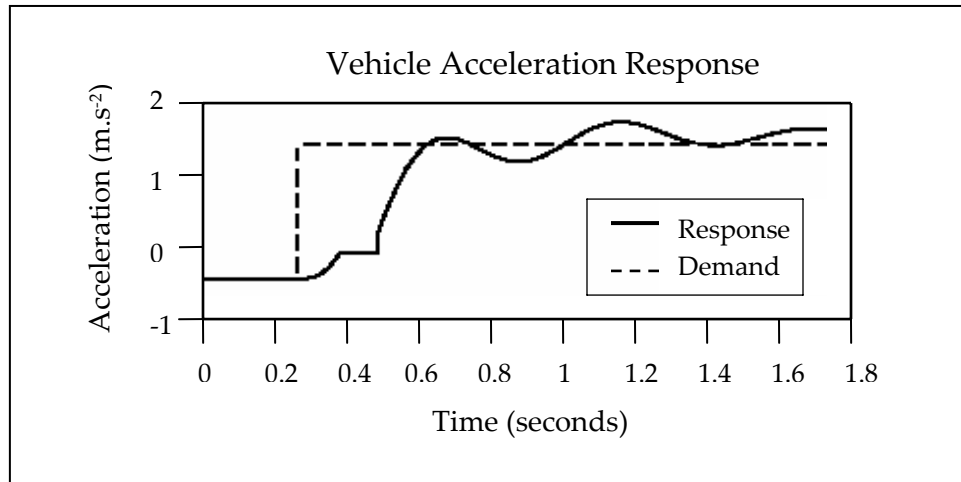


Figure 2.4.3: Simple Switching Control (Lagerberg and Egardt, 2002)

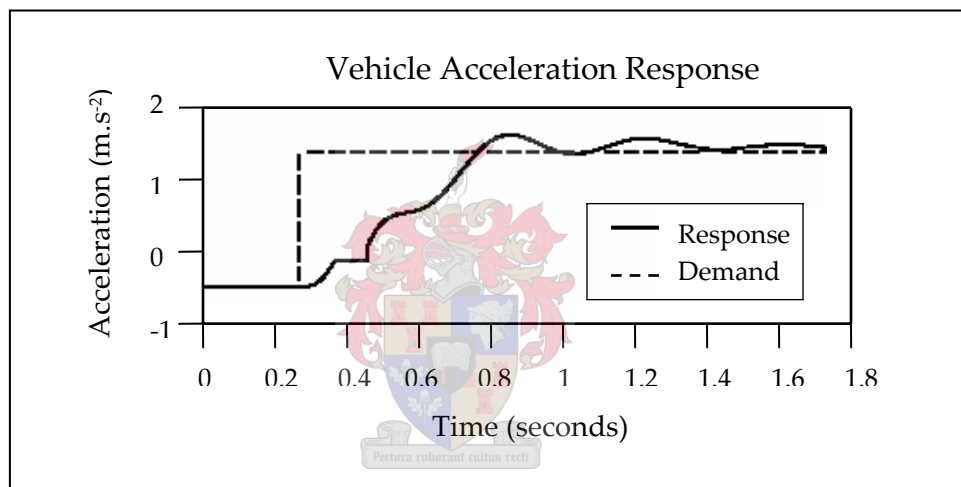


Figure 2.4.4: Modified Switching Control (Lagerberg and Egardt, 2002)

The previously described switching controllers require knowledge of when the drivetrain is in the backlash region so that the backlash control mode can be implemented. Backlash state estimators (observers) were derived for this purpose in Lagerberg and Egardt (2003). Non-linear backlash models and Kalman filtering techniques were used to estimate the backlash size and position. Lagerberg and Egardt (2004) is an experimental verification of the accuracy of these estimates through vehicle testing. It was concluded that the estimates were of a high quality and that they were robust to modelling errors.

# Drivetrain Modelling

# 3

## 3.1 Introduction

The powertrain is defined as everything that propels the car. The drivetrain is the complete powertrain excepting the engine. In other words, the drivetrain comprises of the flywheel, clutch, transmission, driveshafts and wheels.

Figure 3.1.1 shows the major inertias, gear ratios and torques used in the drivetrain model. In this diagram,  $I_f$  and  $\theta_f$  are the flywheel inertia and angular position.  $T_f$  is the engine torque transmitted to the flywheel,  $T_c$  is the drivetrain torque acting on the transmission, and  $\theta_c$  is the angular displacement of the clutch.  $I_t$ ,  $\theta_t$ ,  $i_t$  and  $b_t$  are the transmission inertia, angular position, gear ratio and viscous friction coefficient respectively.  $T_d$  is the driveshaft torque acting on the wheels, while  $I_w$  and  $\theta_w$  are the mass moment of inertia and angular position of each wheel.  $T_t$  is the tractive torque acting on the tyre.

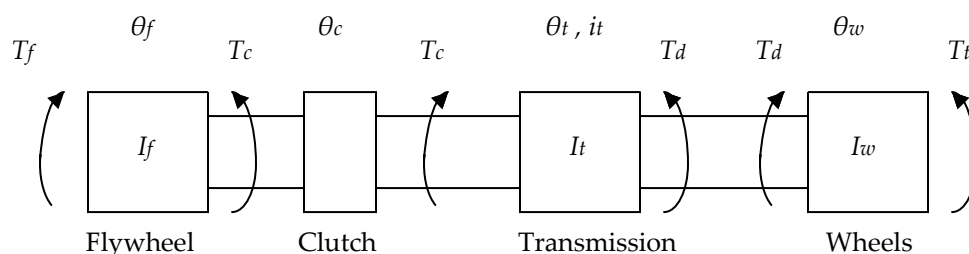


Figure 3.1.1: Drivetrain Inertias



In this chapter a complex non-linear model of the drivetrain is derived. This model was used for advanced vehicle simulations in Chapter 5. Next, the non-linear model was linearized and simplified. The primary purpose of simplifying the model was that it would later simplify the process of controller development. The controller would be developed using this simplified model and the effect of the additional non-linear parameters would later be analyzed. The controller would then be tuned accordingly.

## 3.2 Complex Model

### 3.2.1 Engine, Flywheel and Clutch

Using Newton's second law at the flywheel inertia, the following model is obtained:

$$I_f \cdot \ddot{\theta}_f = T_f - T_c \quad (3.2.1)$$

In order to develop a realistic drivetrain controller, engine dynamics must be considered when calculating  $T_f$ . As described in Lagerberg and Egardt (2002), the engine is modelled as an ideal torque generator with first order dynamics and a simple transport delay. In other words, the assumption is made that the ECU engine torque controller results in the following closed-loop engine dynamics:

$$T_f(s) = \frac{e^{-L_e s}}{t_{eng} \cdot s + 1} u(s) \quad (3.2.2)$$

The torque demand is  $u$  and the time constant and transport delay of the engine are  $t_{eng}$  and  $L_e$  respectively. A maximum engine torque ( $T_{f,max}$ ) is also implemented.

As described in Pettersson (1996), the clutch consists of springs arranged circumferentially around a driven hub. The stiffness of these springs determines how the torque is transmitted from the flywheel to the transmission. As shown in Figure 3.2.1, the clutch torsional stiffness coefficient is  $k_{c1}$  for a deflection angle from 0 to  $\theta_{c1}$ , and  $k_{c2}$  for a deflection angle from  $\theta_{c1}$  to the mechanical stop ( $\theta_{c2}$ ). The torque component due to the clutch torsional stiffness can therefore be described by the following equations:

$$\begin{aligned} \theta_c &= (\theta - \theta_c \cdot i_t) \\ T_c &= \begin{cases} \theta_c \cdot k_{c1} & \text{if } |\theta_c| \leq |\theta_{c1}| \\ \theta_{c1} \cdot k_{c1} + (\theta_c - \theta_{c1}) \cdot k_{c2} & \text{if } |\theta_{c1}| < |\theta_c| < |\theta_{c2}| \\ \theta_{c1} \cdot k_{c1} + (\theta_{c2} - \theta_{c1}) \cdot k_{c2} & \text{if } |\theta_c| \geq |\theta_{c2}| \end{cases} \end{aligned} \quad (3.2.3)$$

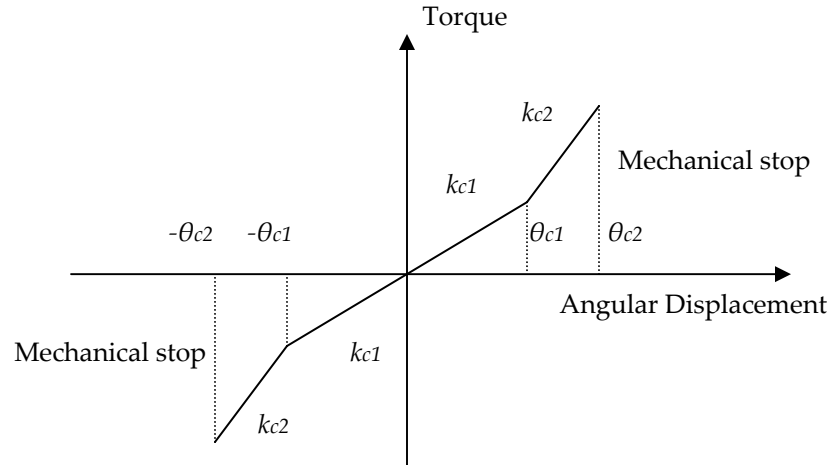


Figure 3.2.1: Clutch Stiffness Coefficient (Pettersson, 1996)

If the clutch damping coefficient is  $c_c$ , the clutch torque component due to damping is:

$$T_{cc} = c_c \cdot \dot{\theta}_c \quad (3.2.4)$$

The overall clutch torque  $T_c$  can therefore be written as:

$$T_c = T_{ck} + T_{cc} \quad (3.2.5)$$

### 3.2.2 Transmission and Driveshaft

The gearbox and differential form one compact transmission assembly in a front-wheel drive car. As in Pettersson (1996), it was assumed that the transmission was infinitely stiff when compared to the clutch. Due to the fact that the drivetrain was being modelled for longitudinal motion in a straight line, both front wheels were propelled at the same speed and the transmission could therefore be modelled as a single inertia and gear ratio. Applying Newton's second law around the transmission inertia (Figure 3.1.1):

$$I_t \cdot \ddot{\theta}_t = T_c \cdot i_t - b_t \cdot \dot{\theta}_t - T_d \quad (3.2.6)$$

The torque in the driveshaft ( $T_d$ ) is a function of the backlash in the drivetrain. Karlsson (2001) defines backlash as the small amount of mechanical slack between adjacent movable components. Each clearance is relatively small, but when they are added together the total backlash limits the system performance. When the torque in the drivetrain changes direction, the backlash changes side and this phenomenon makes it important to include a model of the backlash to achieve realistic simulations.

There are three major backlash models in literature (Lagerberg, 2001): the dead zone model, the modified dead zone model and the complex model. The dead zone model is the most commonly used, but is nevertheless erroneous. If damping is included in this model it can be shown that the backlash can produce a pulling force. The complex model and modified dead zone model have extra states that prevent a pulling force at contact. The complex version relies on parameterized curve descriptions and is not very practical. Karlsson (2001) showed that the modified dead zone model coincides with the more complex version for realistic parameter settings, and it was therefore used to model the backlash in this thesis.

Figure 3.2.2 represents a driveshaft with backlash. The stiffness and damping coefficients of the driveshaft are  $k_s$  and  $c_s$  respectively, and  $\alpha$  is half the backlash angle. The modified dead zone backlash model for the driveshaft torque  $T_d$  is represented by the following equation:

$$\begin{aligned} \theta_{rel} &= \theta_t - \theta_w \\ T_{dz} &= \begin{cases} k_s \cdot (\theta_{rel} - \alpha) + c_s \cdot \dot{\theta}_{rel} & \text{if } \theta_{rel} > \alpha \\ k_s \cdot (\theta_{rel} + \alpha) + c_s \cdot \dot{\theta}_{rel} & \text{if } \theta_{rel} < -\alpha \\ 0 & \text{if } |\theta_{rel}| \leq \alpha \end{cases} \\ T_d &= \begin{cases} 0 & \text{if } T_{dz} < 0 \text{ and } \theta_{rel} > 0 \text{ or if } T_{dz} > 0 \text{ and } \theta_{rel} < 0 \\ T_{dz} & \text{otherwise} \end{cases} \end{aligned} \quad (3.2.7)$$

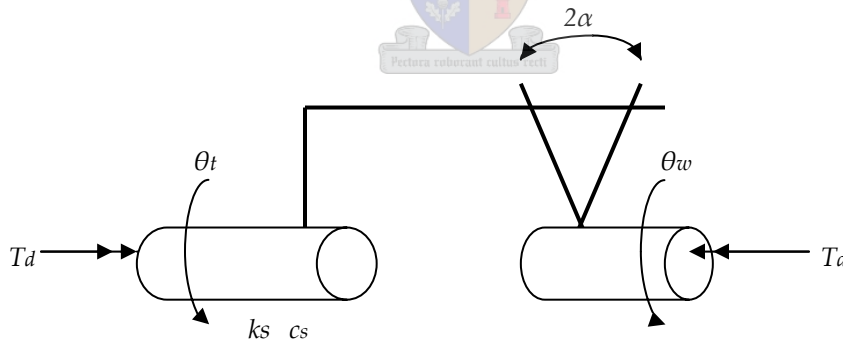


Figure 3.2.2: Driveshaft with Backlash

### 3.2.3 Wheel and Vehicle

$F_t$  is the tractive force on the moving wheel. This force is converted into a torque and Newton's second law is applied around the two driven wheels (Figure 3.1.1):

$$2 \cdot I_w \cdot \ddot{\theta}_w = T_d - r_w \cdot F_t \quad (3.2.8)$$

Figure 3.2.3 shows the longitudinal forces acting on a vehicle with mass  $m$ , velocity  $v$  and wheel radius  $r_w$ . Using Newton's second law in the longitudinal direction, the following equation is obtained:

$$m \cdot \dot{v} = F_t - F_a - F_r - F_g \quad (3.2.9)$$

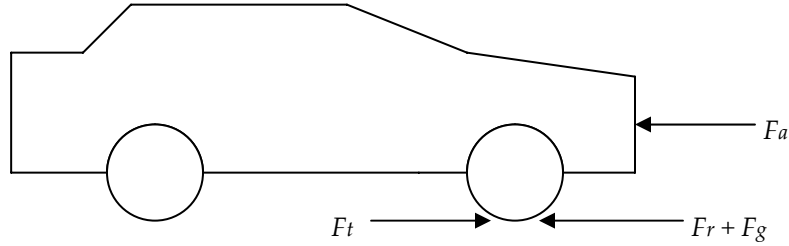


Figure 3.2.3: Longitudinal Forces on a Vehicle

$F_a$  is the air drag force. With the drag coefficient, maximum vehicle cross sectional area and air density represented by  $c_w$ ,  $A$ , and  $\rho$  respectively, the drag force is described by:

$$F_a = \frac{1}{2} \cdot c_w \cdot A \cdot \rho \cdot v^2 \quad (3.2.10)$$

$F_r$  is the rolling resistance force, and it was modelled as in Wong (2001). The speed independent coefficient is  $c_{r1}$  and the speed dependent coefficient is  $c_{r2}$ .

$$F_r = m \cdot g \cdot (c_{r1} + c_{r2} \cdot v^2) \quad (3.2.11)$$

$F_g$  is the gradient force on the vehicle, and for a road with slope  $\beta$  it is described by:

$$F_g = m \cdot g \cdot \sin(\beta) \quad (3.2.12)$$

The friction coefficient between a tyre and the road is a function of the longitudinal slip of the tyre. This slip rate results from a reduction of the effective circumference of the tyre due to the elasticity of the tyre rubber (Canudas-De-Wit et. al., 2003). In this drivetrain model, the tyre is assumed to roll without slip. The vehicle and wheel velocities are now related by:

$$v = r \cdot \dot{\theta} \quad (3.2.13)$$

Re-writing (3.2.9) gives:

$$F_t = m \cdot \dot{v} + F_r + F_a + m \cdot g \cdot \sin(\beta) \quad (3.2.14)$$

Combining (3.2.8), (3.2.13) and (3.2.14) results in:

$$(2 \cdot I_w + m \cdot r^2) \cdot \ddot{\theta}_w = T_d - (F_r \cdot r + F_a \cdot r + m \cdot g \cdot r \cdot \sin(\beta)) \quad (3.2.15)$$

It is important to note that the tyre dynamics result in the majority of the drivetrain damping. These dynamics are accounted for by increasing the damping coefficient of the driveshaft.

### 3.2.4 Summary

In summary, the three principle differential equations representing the drivetrain model are:

$$I_f \cdot \ddot{\theta}_f = T_f - T_c \quad (3.2.1)$$

$$I_t \cdot \ddot{\theta}_t = T_c \cdot i_t - T_d - b_t \cdot \dot{\theta}_t \quad (3.2.6)$$

$$(2 \cdot I_w + m \cdot r^2) \cdot \ddot{\theta}_w = T_d - (F_r \cdot r + F_a \cdot r + m \cdot g \cdot r \cdot \sin(\beta)) \quad (3.2.15)$$

A block diagram overview of the model is shown in Figure 3.2.4. More detailed (lower level) block diagrams can be found in Appendix A.

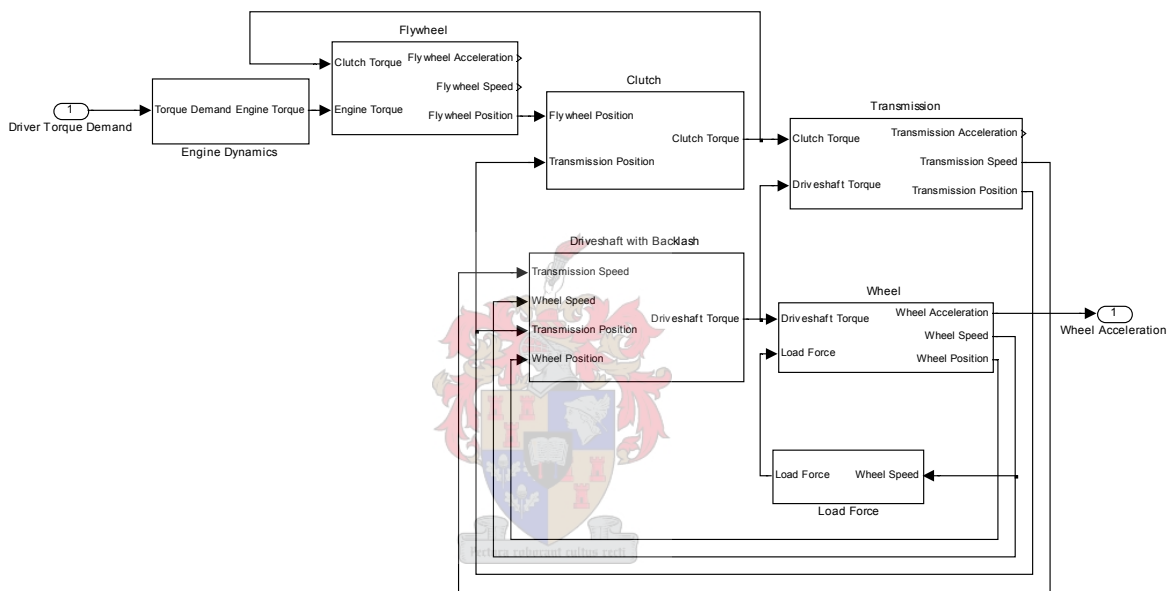


Figure 3.2.4: Complex Model Block Diagram

## 3.3 Simplified Model

For the purpose of reducing the complexity of the controller development process, a simplified linear drivetrain model was derived. This model would enable linear control theory to be applied to the problem of drivetrain control. The effect of the drivetrain non-linearities on the performance of the controller was later analyzed and the controller was then tuned accordingly. The model used in this study was presented in Fredriksson (1999) and additions were made in Fredriksson et. al. (2002). This same drivetrain model was also used in Karlsson (2001).

This simplified model ignores engine dynamics as well as friction in the drivetrain. The transmission inertia is assumed to be negligibly small in comparison to that of

the flywheel and wheels. Due to the transmission gear ratios, the driveshaft has a torque to stiffness ratio several times that of the clutch. The drivetrain dynamics are therefore assumed to dominate, and the clutch is treated as being stiff. Backlash is not accounted for.

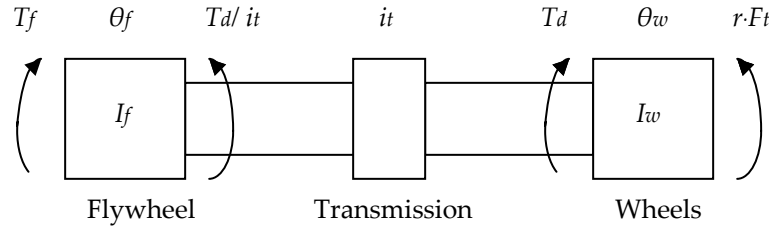


Figure 3.3.1: Simplified Linear Drivetrain Model

Using the same nomenclature as in Section 3.2 and applying Newton's second law around the major inertias (Figure 3.3.1), the following equations result:

$$I_f \cdot \ddot{\theta}_f = T_f - \frac{T_d}{i_t} \quad (3.3.1)$$

$$T_d = \left( k_s \cdot \left( \frac{\theta_f}{i_t} - \theta_w \right) + c_s \cdot \left( \frac{\dot{\theta}_f}{i_t} - \dot{\theta}_w \right) \right) \quad (3.3.2)$$

$$2 \cdot I_w \cdot \ddot{\theta}_w = T_d - r \cdot F_t \quad (3.3.3)$$

The longitudinal forces acting on the vehicle are derived in the same way as they were with the complex model:

$$(2 \cdot I_w + m \cdot r^2) \cdot \ddot{\theta}_w = T_d - (F_r \cdot r + F_a \cdot r + m \cdot g \cdot r \cdot \sin(\beta)) \quad (3.2.15)$$

Combining (3.3.1), (3.3.2) and (3.2.15), the differential equations are written as:

$$I_f \cdot \ddot{\theta}_f = T_f - \left( \frac{k_s}{i_t} \cdot \left( \frac{\theta_f}{i_t} - \theta_w \right) + \frac{c_s}{i_t} \cdot \left( \frac{\dot{\theta}_f}{i_t} - \dot{\theta}_w \right) \right) \quad (3.3.4)$$

$$I_c \cdot \ddot{\theta}_w = k_s \cdot \left( \frac{\theta_f}{i_t} - \theta_w \right) + c_s \cdot \left( \frac{\dot{\theta}_f}{i_t} - \dot{\theta}_w \right) - T_t \quad (3.3.5)$$

The term  $(2 \cdot I_w + m \cdot r^2)$  has been combined as a single inertia  $I_c$ , and the tractive torque  $T_t$  is defined as:

$$T_t = F_r \cdot r + F_a \cdot r + m \cdot g \cdot r \cdot \sin(\beta) \quad (3.3.6)$$

The following three state variables are introduced; the torsion in the driveshaft, the wheel speed and the engine speed:

$$\begin{aligned}
 X_1 &= \left( \frac{\theta}{i_t} - \theta_w \right) \\
 X_2 &= \dot{\theta}_w \\
 X_3 &= \dot{\theta}_f
 \end{aligned} \tag{3.3.7}$$

The drivetrain model can now be written in state space form as:

$$\begin{bmatrix} \dot{X}_1 \\ \dot{X}_2 \\ \dot{X}_3 \end{bmatrix} = \begin{bmatrix} 0 & -1 & \frac{1}{i_t} \\ \frac{k_s}{I_c} & -\frac{c_s}{I_c} & \frac{c_s}{i_t \cdot I_c} \\ -\frac{k_s}{i_t \cdot I_f} & \frac{c_s}{i_t \cdot I_f} & \frac{-c_s}{i_t^2 \cdot I_f} \end{bmatrix} \begin{bmatrix} X_1 \\ X_2 \\ X_3 \end{bmatrix} + \begin{bmatrix} 0 & 0 \\ 0 & -\frac{1}{I_c} \\ \frac{1}{I_f} & 0 \end{bmatrix} \begin{bmatrix} T_f \\ T_t \end{bmatrix} \tag{3.3.8}$$

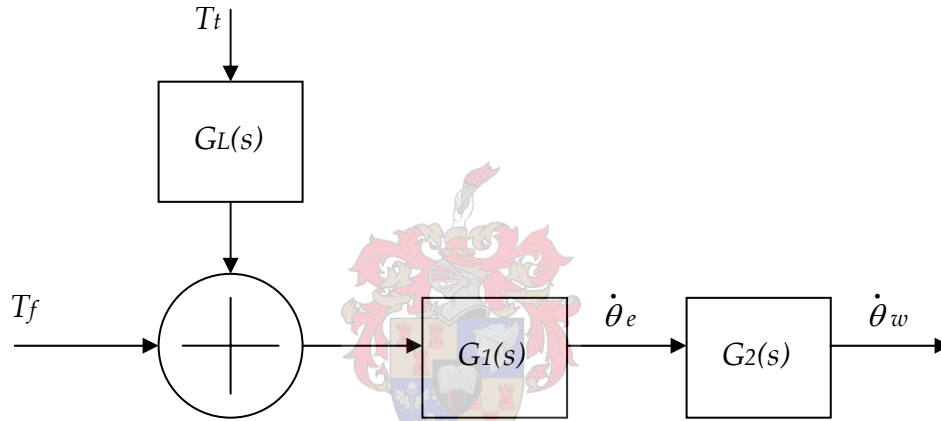


Figure 3.3.2: Block Diagram of the Simplified Model Transfer Functions

Converting the state-space matrices of (3.3.8) into transfer functions yields the following (Figure 3.3.2):

$$G_1(s) = \frac{\frac{1}{I_f} s^2 + \frac{c_s}{I_f \cdot I_c} s + \frac{k_s}{I_f \cdot I_c}}{s^3 + \left( \frac{c_s}{I_c} + \frac{c_s}{I_f \cdot i_t^2} \right) s^2 + \left( \frac{k_s}{I_c} + \frac{k_s}{I_f \cdot i_t^2} \right) s} \tag{3.3.9}$$

$$G_2(s) = \frac{\frac{c_s}{i_t \cdot I_f \cdot I_c} s + \frac{k_s}{i_t \cdot I_f \cdot I_c}}{\frac{1}{I_f} s^2 + \frac{c_s}{I_f \cdot I_c} s + \frac{k_s}{I_f \cdot I_c}} \tag{3.3.10}$$

$$G_L(s) = \frac{\frac{-c_s}{i_t \cdot I_f \cdot I_c} s - \frac{k_s}{i_t \cdot I_f \cdot I_c}}{\frac{1}{I_f} s^2 + \frac{c_s}{I_f \cdot I_c} s + \frac{k_s}{I_f \cdot I_c}} \tag{3.3.11}$$

The transfer function of engine torque to driveshaft torque is:

$$G(s) = \frac{\frac{c_s}{i_t \cdot I_f} s + \frac{k_s}{i_t \cdot I_f}}{s^2 + \left( \frac{c_s}{I_c} + \frac{c_s}{I_f \cdot i_t^2} \right) s + \left( \frac{k_s}{I_c} + \frac{k_s}{I_f \cdot i_t^2} \right)} \quad (3.3.12)$$

$G(s)$  is a second-order system and its denominator therefore has the form:

$$s^2 + \left( \frac{c_s}{I_c} + \frac{c_s}{I_f \cdot i_t^2} \right) s + \left( \frac{k_s}{I_c} + \frac{k_s}{I_f \cdot i_t^2} \right) = s^2 + 2 \cdot \zeta \cdot \omega_n \cdot s + \omega_n^2 \quad (3.3.13)$$

$\zeta$  and  $\omega_n$  are the damping ratio and natural frequency of the system respectively. The natural frequency of the drivetrain oscillations (shuffle frequency) can therefore be written as:

$$\omega_n = \sqrt{\left( \frac{k_s}{I_c} + \frac{k_s}{I_f \cdot i_t^2} \right)} \quad (3.3.14)$$

This shows that the shuffle frequency is only dependent on the driveshaft stiffness, flywheel inertia, gear ratio, wheel inertia, wheel radius and vehicle mass.





# Parameter Identification

# 4

## 4.1 Introduction

This chapter describes the procedures used to identify the drivetrain model parameters. The values chosen for each component are then summarized. Parameter values were obtained through experimentation on a test-rig, analysis of vehicle measurement data, or simply by referencing. Table 4.1.1 indicates which of the procedures was used for each of the parameters.

Table 4.1.1: Experimental Procedures

Backlash angle	Experimentation
Driveshaft stiffness	Experimentation
Friction	Experimentation
Gear ratios	Experimentation
Inertias	Experimentation
Drivetrain damping	Vehicle measurement data
Clutch stiffness	Referenced
Other	Referenced

## 4.2 Experimental Apparatus

### 4.2.1 Test-Rig

A test-rig was designed and manufactured to mount the drivetrain on a large direct current (DC) electric motor. A Siemens Simoreg (K-type) variable speed

drive (VSD) was used to accurately control the speed and torque output of the motor. This motor control, coupled with accurate speed measurements at several places along the drivetrain, generated data which enabled the characterisation of several drivetrain components. Figure 4.2.1 is a schematic of the experimental setup and Figure 4.2.2 shows the assembled test-rig. (More detail on this rig can be found in Appendix B.)

The motor was mounted on four leaf springs which, if extended, would intersect the motor axis. These mounts therefore did not apply any moment on the motor frame, and any reaction torque on the frame was sensed by the load cell which was connected between the frame and test bed.

A shaft with universal joints was used to connect the flywheel and motor. This shaft was the only component on the experimental setup that differed from the actual drivetrain assembly in the car. The flywheel transferred torque from this shaft to the transmission through the clutch, which was permanently engaged. The transmission included the gearbox and differential. The latter was locked to ensure that both wheels would be driven at the same velocity. A single driveshaft was in turn connected to the differential, and the wheel and brake disk assembly was connected to this driveshaft.

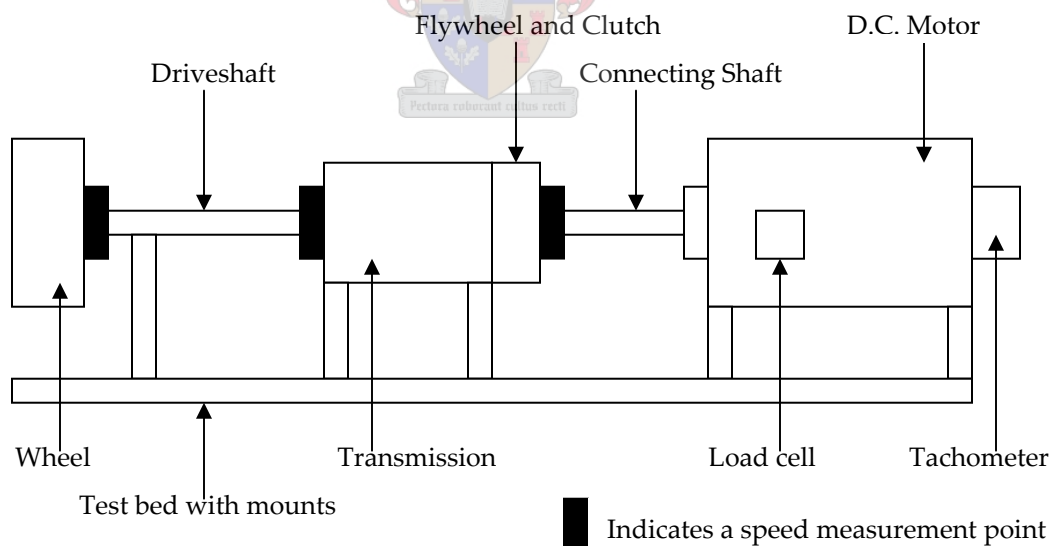


Figure 4.2.1: Experimental Setup



Figure 4.2.2: Fully Assembled Test-Rig

## 4.2.2 Sensors

### 4.2.2.1 Torque

The load cell used to measure the torque was attached between the motor frame (which was free to rotate) and the test-rig base (Figure 4.2.3). The voltage output of the load cell was directly proportional to the force exerted on it by the rotation of the motor frame. Since the angle of rotation of the frame was miniscule, the distance from the centre of rotation to the load cell was approximately constant, and the voltage was therefore also directly proportional to the reaction torque on the motor.



Figure 4.2.3: The Load Cell Setup

The load cell signal was passed through a bridge amplifier which converted it into a -5 to +5 V signal. The load cell torque value and the torque acting on the drivetrain were related as follows:

$$T_{Load\ Cell} = T_{Drivetrain} + I_{Motor} \cdot \ddot{\theta}_{Motor} \quad (4.2.1)$$

The load cell was calibrated before each test by hanging various known weights on a 0.649 m torque arm. A linear scaling formula relating the measured voltages and their relative torque values was calculated. This formula was used to scale all voltages measured during testing to torque values.

#### 4.2.2.2 Speed

The motor speed was measured using a tachometer which provided a voltage proportional to its rotational speed. This voltage was passed through the variable speed drive which in turn converted it into a -10 to +10 V signal. The signal was then converted to speed (in rpm) using the following formula:

$$Speed(rpm) = 554.18 \cdot V + 4.613 \quad (4.2.2)$$

Other speed measurements were made at the flywheel, after the gearbox, and at the wheel using 120-tooth disks and digital magnetic pickups (Figure 4.2.4). The disks were attached along the axis of rotation of the drivetrain so that they rotated at the same rate as the component at which the measurement was being made. The pickups provided a 0 – 5 V digital (square wave) signal representing the rising and falling edges of the disk teeth. The processing of this signal is further described in Section 4.3.2.



Figure 4.2.4: Digital Magnetic Pick-up Speed Measurement

## 4.3 Data Acquisition

### 4.3.1 Analogue Signals

The load cell and tachometer provided analogue voltage signals of the motor torque and speed respectively. Various other analogue voltage waveforms were also used as inputs to the Siemens VSD, which in turn ensured that the motor followed these signals. A National Instruments PCI-6014 data acquisition (DAQ) card was used to measure all analogue input signals as well as to generate all analogue output signals. The program used to control the DAQ card was written in Borland C++ since all the relevant National Instruments drivers supported this language.

With regards to the chosen sampling times, Franklin et al. (2002) suggests that a sample rate of 20 to 40 times the system's closed loop bandwidth should be used. Conradie (2001) determined that the maximum closed loop bandwidth of the motor was 5.33 Hz, and it was therefore decided that a sample rate of 200 Hz would be an appropriate choice.

### 4.3.2 Digital Signals

This form of data acquisition was applied to the speed measurements made using the digital magnetic pick-ups. A National Instruments PCI-6602 counter-timer card was programmed (again using Borland C++) to count the number of pulses produced by its onboard 20 MHz oscillator clock between successive rising edges in the pick-up's signal. The time taken for the toothed-disk to rotate between successive teeth could then be calculated using the correlation:

$$Time(s) = Counts / 20000000 \quad (4.3.1)$$

For a disk with 120 teeth the speed was calculated using:

$$Speed(rpm) = \left( \frac{Time \cdot 120}{60} \right)^{-1} \quad (4.3.2)$$

In this way a speed reading was obtained every 3°.

The maximum motor speed used was 5000 rpm and the fastest tooth period was therefore 0.0001 seconds. This corresponded to a minimum of 2000 oscillator clock pulses per tooth period. The nature of the counter operation is such that 1999, 2000 or 2001 pulses could be counted depending on when counting was started. The worst resolution of the counting operation was therefore  $1/2000 = 0.05\%$ .

## 4.4 Experimental Procedures

This section describes the experimental procedures used to determine the various drivetrain parameters. The results of these experiments are summarized in Section 4.5 for each drivetrain component.

### 4.4.1 Inertia

The mass moment of inertia of each drivetrain component around its axis of rotation was determined by driving the motor with triangular speed functions (in other words constant accelerations). To obtain the average acceleration, a regression of the speed data was performed to obtain the gradient of the line. The reaction torque on the load cell was measured and the average acceleration and torque values were then substituted into the formula:

$$I = \frac{T}{\ddot{\theta}} \quad (4.4.1)$$

Data from an inertia experiment is shown in Figure 4.4.1. The experiment was completed on the test-rig with the drivetrain assembled up to and including the transmission. The DC motor was accelerated and decelerated at approximately 40 rad.s<sup>-2</sup>.

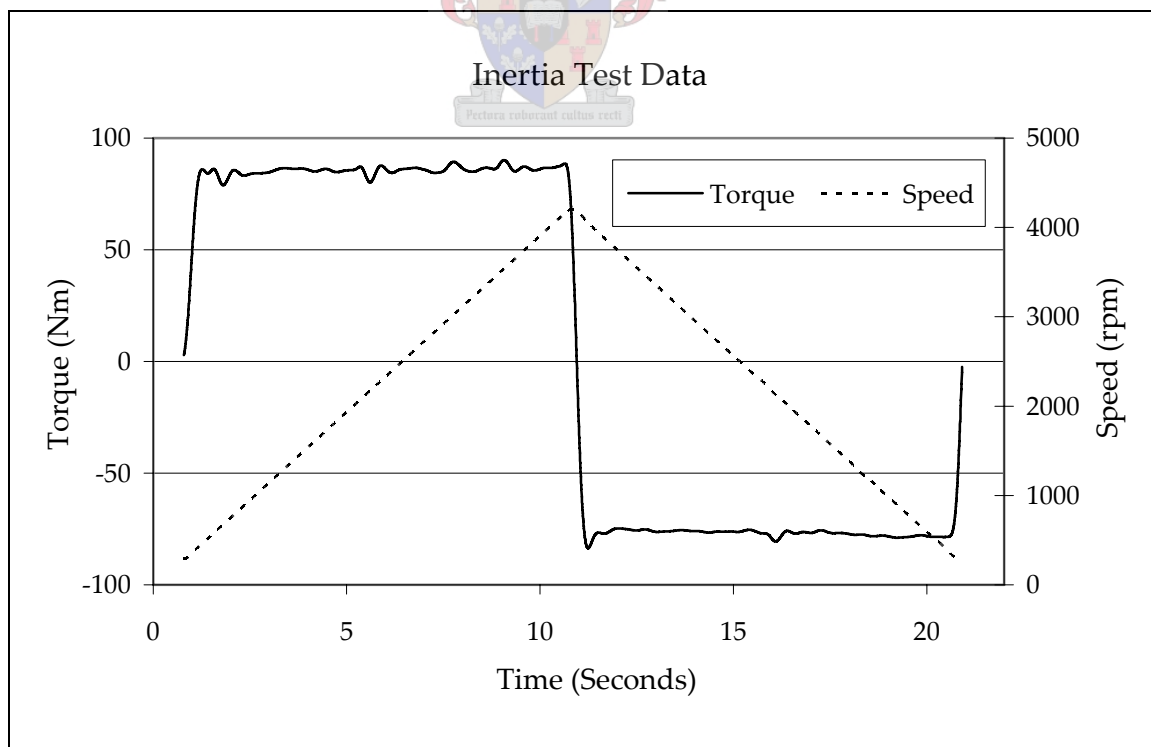


Figure 4.4.1: Inertia Test Data

The inertia of the unloaded electric motor was calculated and the drivetrain was then progressively assembled. A full set of inertial experiments was completed as each new drivetrain component was added. By subtracting the system inertia obtained with the new component attached from the value obtained before the component was attached, the inertia of the extra component could be calculated.

Friction in the system resulted in a reaction torque measurement that was slightly too low during deceleration and slightly too high during acceleration. The mean torque from each speed wave period was therefore calculated by averaging the absolute torque values measured during acceleration and deceleration.

#### 4.4.2 Friction

It was assumed that the friction in the drivetrain was primarily due to the transmission. This friction was assumed to be viscous and is represented by the following equation:

$$T = b \cdot \dot{\theta} \quad (4.4.2)$$

The drivetrain was driven at constant speeds and the average torque values were measured. A straight line was then fitted to the torque versus speed data and the gradient of this straight line was used as the friction coefficient  $b$ . Test data from a friction experiment on the test-rig is shown in Figure 4.4.2. The drivetrain was once again assembled up to and including the transmission (with 5<sup>th</sup> gear engaged). A linear trendline has been fitted to the data.

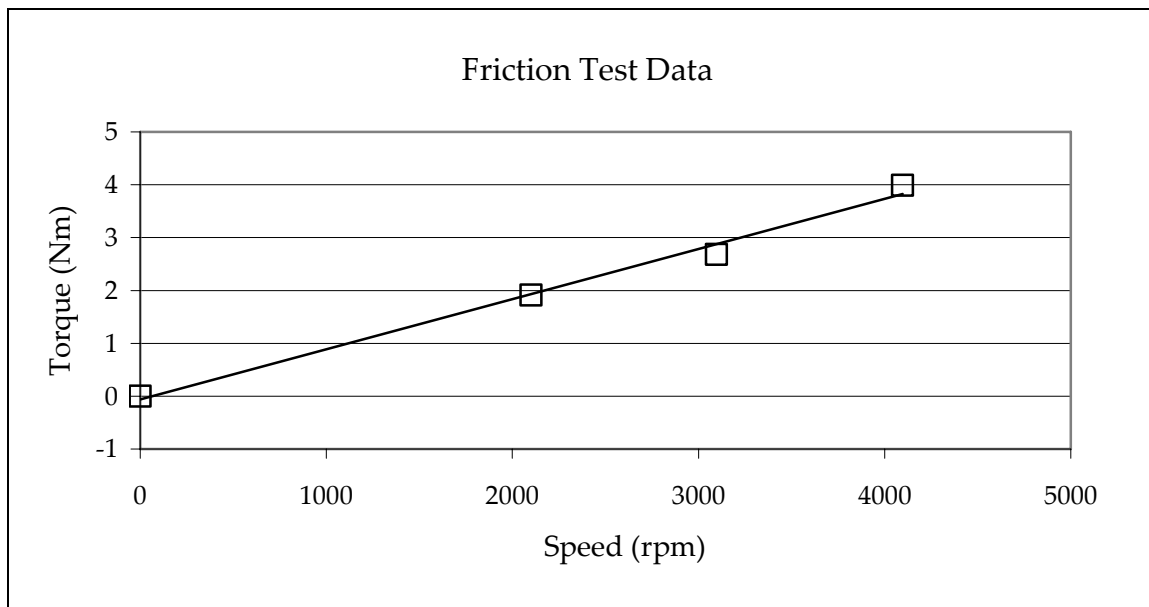


Figure 4.4.2: Friction Test Data

### 4.4.3 Stiffness

Figure 4.4.3 is a schematic of how the stiffness experiments were conducted. One end of the drivetrain component was fixed while a torque moment was applied to the other end. The magnitude of the torsional moment was equal to the product of the hanging weight and the torque arm length.

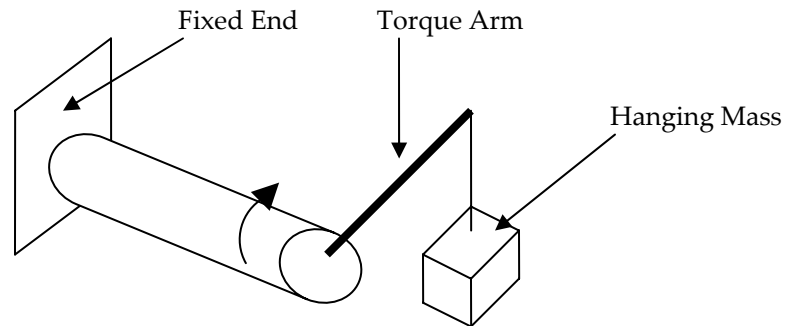


Figure 4.4.3: Stiffness Experiment

The angular deflection of the component was measured on the free end and the experiment was repeated for various loads. A linear regression was performed on the torque versus deflection data and the gradient of the resulting straight line was the stiffness of the component. This is described by:

$$k = \frac{T}{\theta} \quad (4.4.3)$$

Test data from a clutch stiffness experiment (Maree, 2005) is shown in Figure 4.4.4.

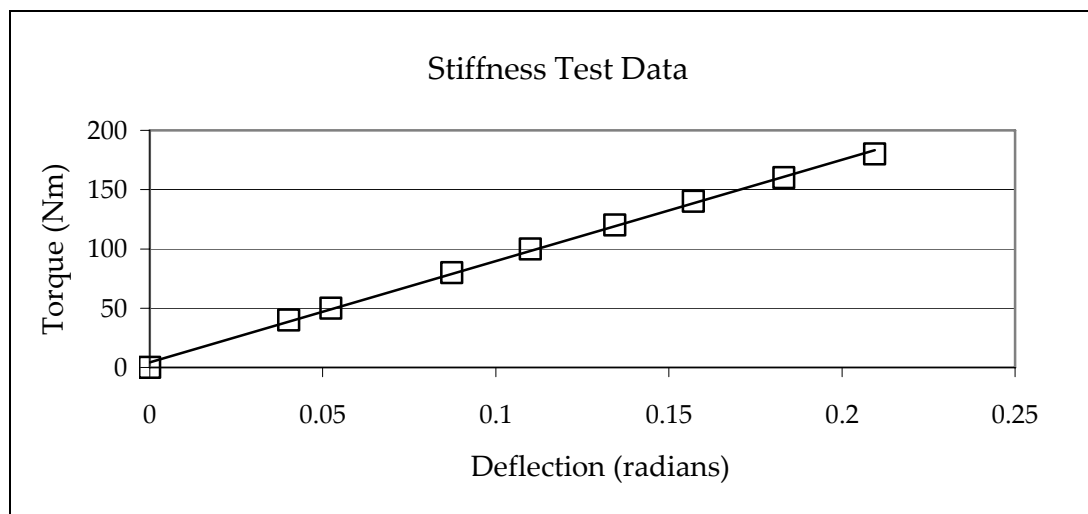


Figure 4.4.4: Stiffness Test Data (Maree, 2005)



#### 4.4.4 Damping

Vehicle behaviour was simulated for changes in engine torque and gear-changing was ignored. The clutch was therefore always engaged and the assumption was made that there was no slip between the clutch and flywheel. This allowed the drivetrain damping due to the clutch, driveshaft and tyre to be combined as a single drivetrain damping coefficient ( $c_s$ ) which was applied at the driveshaft. The value used is discussed in Section 4.5.6.

### 4.5 Results

#### 4.5.1 D.C. Motor

Although the motor did not form part of the drivetrain model, it was necessary to characterise it so as to identify the drivetrain parameters. As previously mentioned, the motor was controlled by a VSD, and the unloaded closed-loop DC motor system had the following parameters:

Table 4.5.1: DC Motor Parameters

Speed Range	0 – 5500 rpm
Maximum Acceleration	4800 rpm.s <sup>-1</sup>
Inertia	1.76 kg.m <sup>2</sup>

The bandwidth of a system is a measure of the highest input signal frequency that it can follow accurately. Due to the fact that the motor has a large rotational inertia and limited power, its bandwidth will be highly dependent on the speed and amplitude of the oscillations. Figure 4.5.1 shows the closed-loop bandwidth of the motor for various speeds and amplitudes as obtained by Conradie (2001). For these tests, the cut-off frequency was defined as the frequency at which the magnitude of the output signal was 3 dB less than the magnitude of the input signal.

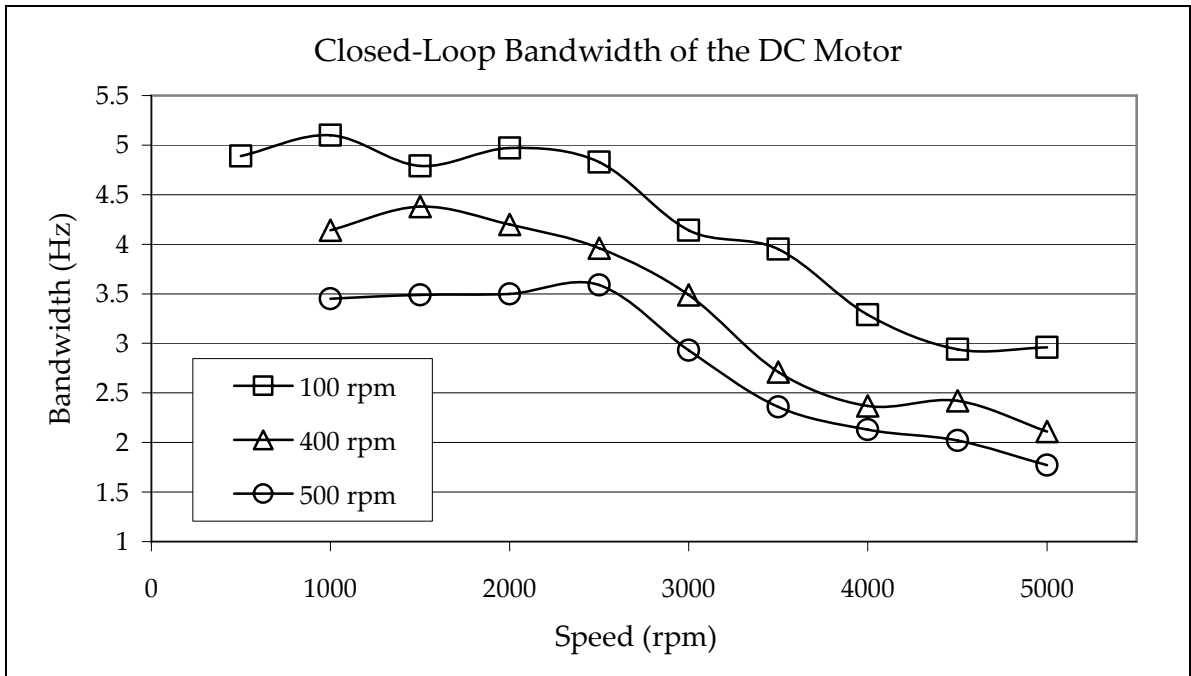


Figure 4.5.1: DC Motor Closed-Loop Bandwidth for Different Speed Amplitudes (After Conradie, 2001)

## 4.5.2 Engine

The engine modelled was a 1.6 litre normally aspirated 4-cylinder spark-ignition engine. As previously stated, it was modelled as having first-order dynamics and a time delay (lag). The maximum transport delay was calculated as the sum of the following delays:

1. The time taken for the pressure rise to be transported from the throttle body to the inlet valve after a step change in throttle position; 0.0015 seconds. This was calculated assuming that the pressure front travelled at the speed of sound ( $345.9 \text{ m.s}^{-1}$  at atmospheric conditions), and that the manifold length was 0.5 m.
2. The time taken for a single inlet and a compression stroke (1 revolution). This is the time taken between the air entering the cylinder and the start of the torque generation (combustion stroke). The assumption is made that if the pressure wave arrives at the inlet valves of a cylinder just after they have closed, it will immediately pass through the inlet valves of the next cylinder which are open.

The maximum total transport delay for the engine is therefore 0.0015 seconds plus 1 full revolution. If the engine speed is 3000 rpm, the lag is:

$$L_e = 0.0015 + 1 \cdot \left( \frac{3000}{60} \right)^{-1} = 0.0215 \text{ seconds} \quad (4.5.1)$$

The time constant of a first-order system is the time taken to reach 63.2% of its steady-state value (Franklin et. al., 2002). It is assumed that if the torque generation begins at the start of the combustion stroke, the maximum torque point is reached by the end of the stroke. In other words ignoring the time delay, the steady-state torque value is reached after 0.5 revolutions. The time constant for the engine at 3000 rpm is therefore:

$$T_{eng} = 0.632 \cdot 0.5 \cdot \left( \frac{3000}{60} \right)^{-1} = 0.00632 \text{ seconds} \quad (4.5.2)$$

The engine torque response to a desired input is shown in Figure 4.5.2.

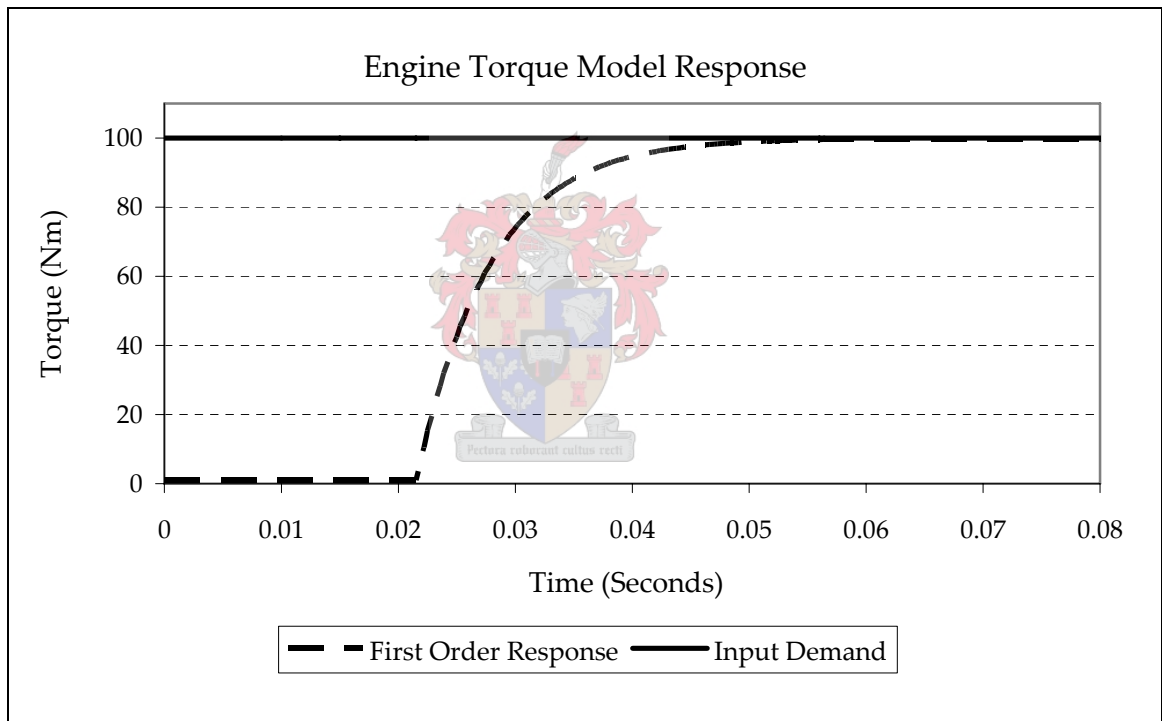


Figure 4.5.2: Engine Torque Model Response

The maximum engine torque for the engine ( $T_{f,max}$ ) was taken as 150 Nm.

### 4.5.3 Flywheel

The flywheel inertia ( $I_f$ ), with the clutch and pressure plate attached, was measured as 0.17 kg.m<sup>2</sup>. To validate this result the flywheel was approximated as a

circular disk. The analytical formula for the mass moment of inertia of a circular disk is given in Hibbeler (1997) as:

$$I = \frac{1}{2} \cdot m \cdot r^2 \quad (4.5.3)$$

The flywheel had an outer radius of 0.15 m and a mass of 15.2 kg. Substituting these values into (4.5.2) an inertia of  $I = 0.171 \text{ kg}\cdot\text{m}^2$  is obtained. This value is almost identical to the experimentally determined value.

#### 4.5.4 Clutch

As described in Chapter 2, the clutch has a torsional stiffness coefficient  $k_{c1}$  for a deflection angle from 0 to  $\theta_{c1}$ , and  $k_{c2}$  for a deflection angle from  $\theta_{c1}$  to the mechanical stop. Maree (2005) showed that the clutch had the following parameters:

Table 4.5.2: Clutch Parameters

$\theta_{c1}$	12° (0.2094 rad)
Maximum Deflection (Mechanical Stop)	14° (0.2443 rad)
$k_{c1}$	854.3 N.m.rad <sup>-1</sup>
$k_{c2}$	1672.2 N.m.rad <sup>-1</sup>

#### 4.5.5 Transmission

The transmission consisted of a 5-speed manual gearbox and differential. Since the drivetrain was a front-wheel drive model, the gearbox and differential formed one compact assembly. The values tabulated below are values measured for the complete assembly.

Table 4.5.3: Transmission Parameters

	Gear Ratio ( $i_t$ )	Friction Coefficient ( $b_t$ )
Gear 1	12.98	0.003 N.m.s.rad <sup>-1</sup>
Gear 2	7.65	0.004 N.m.s.rad <sup>-1</sup>
Gear 3	5.16	0.006 N.m.s.rad <sup>-1</sup>
Gear 4	4.06	0.007 N.m.s.rad <sup>-1</sup>
Gear 5	3.30	0.008 N.m.s.rad <sup>-1</sup>
Reverse	12.02	0.003 N.m.s.rad <sup>-1</sup>

The inertia of the transmission ( $I_t$ ) was measured as  $0.014 \text{ kg.m}^2$ . Although this inertia was far smaller than the dominant flywheel and wheel inertias, it was included in the complex drivetrain model so as to provide a simple means of including the clutch properties.

#### 4.5.6 Driveshaft

The inertia of the driveshaft was measured as  $0.031 \text{ kg.m}^2$ . This inertia was negligibly small when compared to the inertias of the flywheel and wheel.

The measured driveshaft stiffness ( $k_s$ ) was  $6420 \text{ N.m.rad}^{-1}$ , and vehicle measurement data (Momberg, 2005) suggested an overall drivetrain damping coefficient ( $c_s$ ) of  $90 \text{ N.m.s.rad}^{-1}$ . This value was calculated by iteratively changing the damping coefficient parameter in the drivetrain model until the modelled and measured data correlated well. Section 5.4 further discusses the vehicle testing procedures and compares the measured and modelled data in more detail.

The backlash in the drivetrain was measured by locking one end of the drivetrain and measuring the angle of rotational movement (slack) on the other end. The total backlash angle ( $2\alpha$ ) was measured as  $4.5^\circ$ .

#### 4.5.7 Wheel and Brake-Disk

The inertia of a single wheel and tyre was measured as  $0.93 \text{ kg.m}^2$ . Summating this with the brake-disk inertia ( $0.07 \text{ kg.m}^2$ ), the total wheel assembly inertia ( $I_w$ ) was  $1.00 \text{ kg.m}^2$ . The outer radius of the wheel and tyre ( $r_w$ ) was  $0.32 \text{ m}$ .

After a series of vehicle tests on various passenger cars, Wong (2001) suggested average rolling resistance coefficients of  $c_{r1} = 0.0136$  and  $c_{r2} = 5.18 \times 10^{-7}$ .

#### 4.5.8 Vehicle

The vehicle's maximum cross-sectional area ( $A$ ) was measured as  $2.25 \text{ m}^2$ . The mass of the vehicle ( $m$ ) was  $1400 \text{ kg}$ . A typical value for the drag coefficient of modern day vehicles ( $c_w$ ) is  $0.3$  (White, 1999).

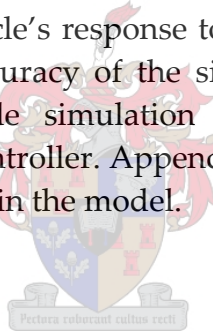
# System Simulation

---

# 5

## 5.1 Introduction

In this chapter, a Simulink / Matlab model of the drivetrain (Appendix A) is generated to simulate the vehicle's response to various torque inputs. The results are then analyzed and the accuracy of the simulations is verified. This process results in an accurate vehicle simulation tool which can be used in the development of a drivetrain controller. Appendix C provides a tabulated summary of the various parameters used in the model.



## 5.2 Working Points

Two scenarios were considered in the vehicle simulations and controller development. The first was the situation where the engine torque output was ramped from 10 Nm to 90 Nm in 0.1 seconds. This could occur when the driver is initially accelerating slowly, and then chooses to rapidly increase the acceleration of the vehicle. It was assumed that the throttle position followed the pedal position (or driver demand) instantaneously. In this scenario the drivetrain does not pass through the backlash region, and any shunt and shuffle that occurs is caused by the driveshaft dynamics.

The second scenario considered was a torque ramp from -10 Nm to 70 Nm in 0.1 seconds. This typically occurs when the throttle is closed (the car is initially decelerating due to the reaction torque by the road on the wheel), and the driver then chooses to rapidly accelerate the vehicle. In this case, the drivetrain passes through the backlash region as the torque changes sign.

The gear ratios in the transmission reduce the engine speed and increase the torque. For example, if the engine speed and torque are 3000 rpm and 100 Nm respectively, a gear ratio of 12.98 (first gear) will result in a wheel speed of  $3000/12.98 = 231.12$  rpm and a driveshaft torque of  $12.98 \times 100 = 1298$  Nm. Because higher gear ratios result in higher driveshaft torque values, the shunt and shuffle is worse in the lower gears. All simulations were therefore performed in first gear unless otherwise stated.

## 5.3 Simulations

### 5.3.1 Complex vs. Simplified Model

The acceleration responses of the complex and simplified models are compared for both working points. The main differences between the models are that the simplified model ignores the clutch dynamics and does not account for backlash, whereas the complex model includes both.

Figure 5.3.1 compares the two models when the drivetrain doesn't pass through the backlash region (in other words for the 10 Nm to 90 Nm torque ramp).

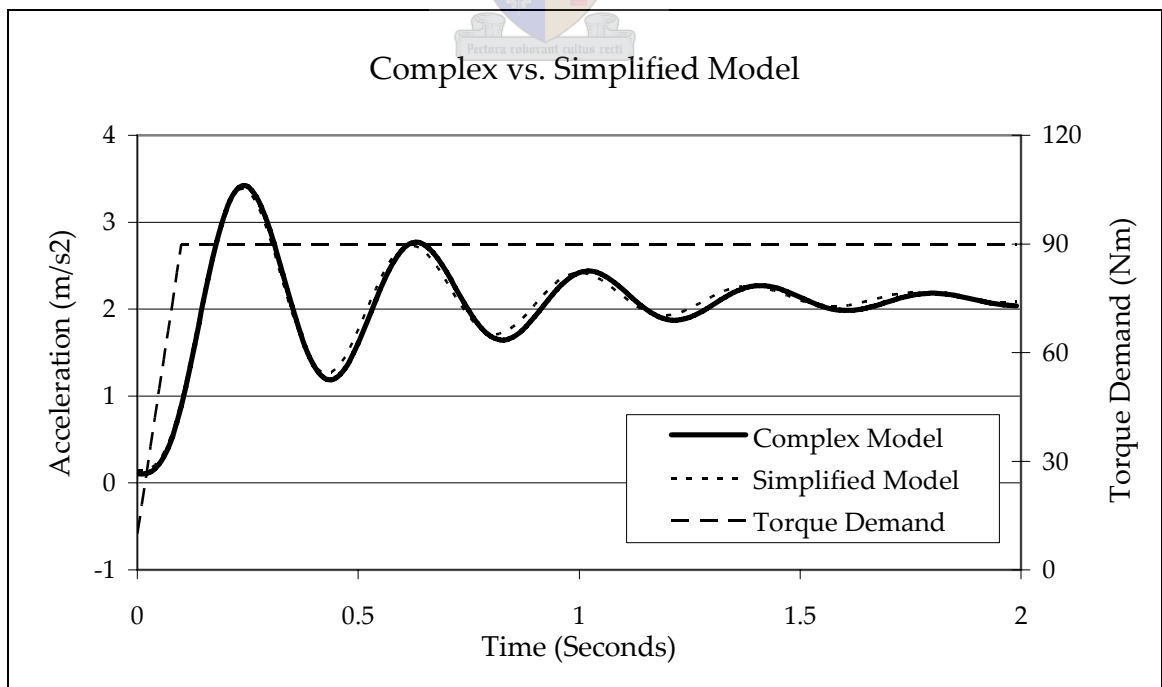


Figure 5.3.1: Complex vs. Simplified Model (10 Nm to 90 Nm Torque Ramp)

It is clear that the response is almost identical for both the complex and simple models. This is to be expected as the main difference between the models is the backlash dynamics, and the backlash region is completely avoided. Since the linear model ignores the clutch dynamics and the complex model includes them, these results also prove that the driveshaft stiffness dominates. This is explained by the fact that the torque to stiffness ratio with the first gear gearing is higher in the driveshaft than in the clutch. It is therefore clear that if the region around negative torque is avoided, the simplified model represents the vehicle behaviour well.

When the second scenario is simulated (a torque input from -10 Nm to 70 Nm), the linear model doesn't compare as well to the complex model. This is due to the fact that the drivetrain now passes through the backlash region (Figure 5.3.2). It is interesting to note that the frequency of the oscillations (shuffle) is still the same for both models ( $\approx 2.6$  Hz in first gear). This once again confirms that the driveshaft stiffness is the dominant drivetrain stiffness.

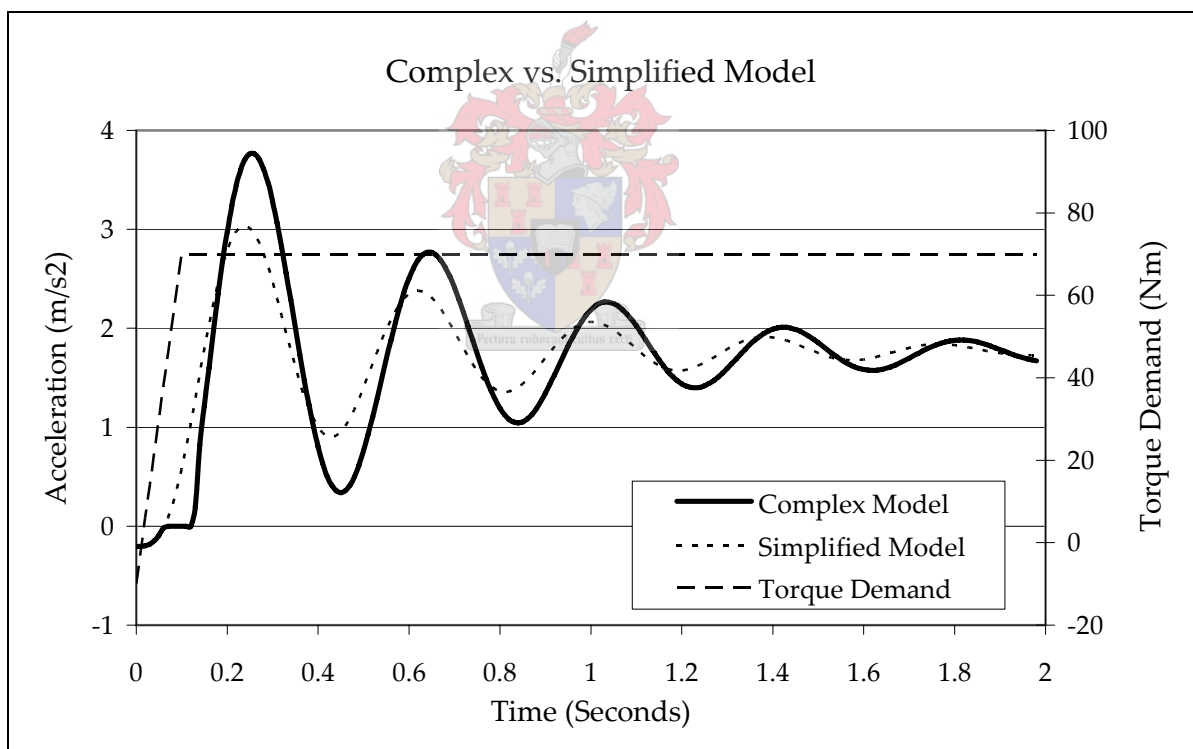


Figure 5.3.2: Complex vs. Simplified Model (-10 Nm to 70 Nm Torque Ramp)



### 5.3.2 Effect of Gear Ratio

The vehicle behaviour in the different gears is now analyzed using the complex drivetrain model. Figure 5.3.3 shows the acceleration responses to a torque ramp from -10 Nm to 70 Nm in gears 1 to 5.

It is clear that the percentage overshoot (shunt) as well as the amplitude of the oscillations (shuffle) decreases as the gear ratio decreases. The shunt and shuffle phenomena are therefore far less apparent in the higher gears. The frequency of the oscillations increases in higher gears.

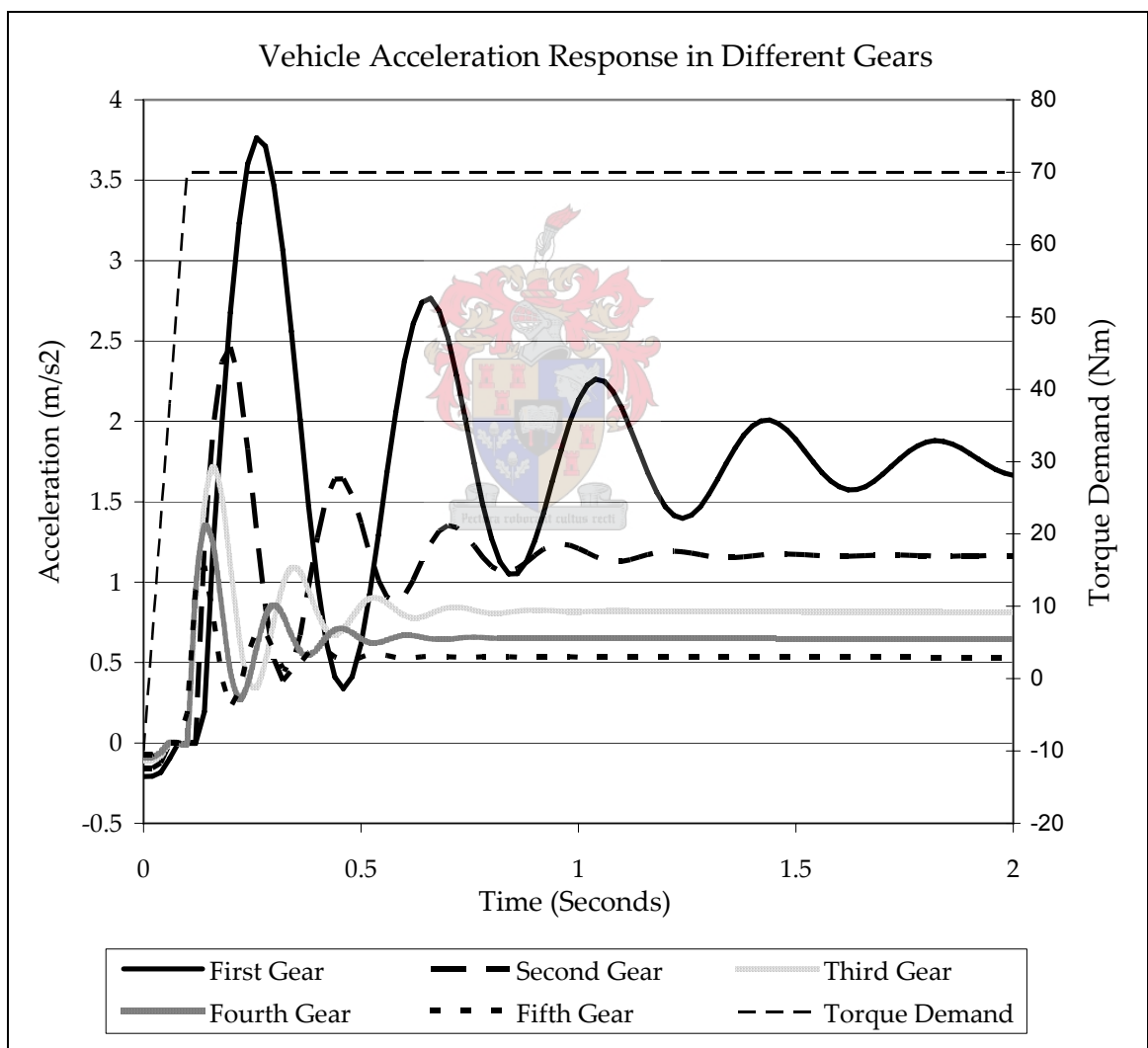


Figure 5.3.3: Vehicle Acceleration Response in Different Gears

## 5.4 Verification of Simulation Accuracy

The accuracy of the models and their resulting vehicle simulations was verified in two ways. Firstly, the results obtained from the simulations were compared to published results of similar simulations. Secondly, measurements were made on an actual vehicle to validate the model.

### 5.4.1 Published Results

In Karlsson (2001) similar simulations were carried out on a Volvo passenger car. The performance of a complex model (including backlash) was also compared to a simplified linear model. Figures 2.3.1 and 2.3.2 show Karlsson's results. As in the current study, Karlsson's complex and simplified models performed equally well when the backlash region was avoided, and the simplified model became unreliable when the drivetrain passed through the backlash region. This confirms that the differences in the responses of the complex and simple models predicted by the simulations in the current study are indeed accurate.

The first gear oscillation frequency obtained by Karlsson (2001) was approximately 3 Hz, and the percentage overshoot when the drivetrain passed through the backlash region was approximately 113%. In the current study, values of 2.6 Hz and 123.9% were obtained. Although these values cannot be directly compared due to the fact that different drivetrains were modelled, the fact that they are quite similar is encouraging.

### 5.4.2 Vehicle Measurements

Measurement data from tests done on a 1.6 litre Volkswagen Jetta (Momberg, 2005) was used to validate the accuracy of the drivetrain model. Momberg fitted an accelerometer to the vehicle in order to measure the longitudinal acceleration, and shunt and shuffle were induced by rapidly accelerating and decelerating the vehicle in second gear. The ECU had algorithms that estimated the torque at the flywheel, and these values were also recorded. A set of test data therefore consisted of the torque estimation as well as the resulting vehicle acceleration.

In the current study, the estimated torque obtained by Momberg was used as the torque input to the complex drivetrain model. The results obtained in the simulation were compared to the measured accelerometer data obtained in

Momberg's vehicle tests. Before a direct comparison could be made however, the accelerometer data had to be digitally filtered. Since the shuffle oscillations were expected to be smaller than 5 Hz, a cut-off frequency of 6 Hz was used. The raw (un-filtered) accelerometer test data is shown in Figure 5.4.1.

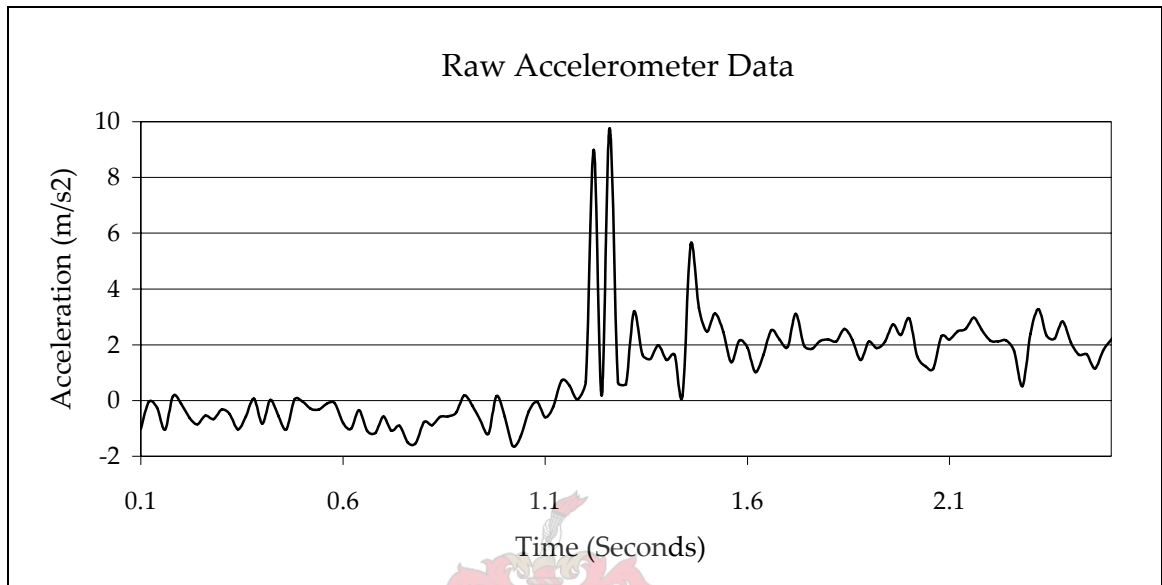


Figure 5.4.1: Raw Accelerometer Test Data

The estimated torque data from the ECU is shown in Figure 5.4.2. The backlash region is evident for the period between 1.06 and 1.1 seconds when the torque is approximately zero.

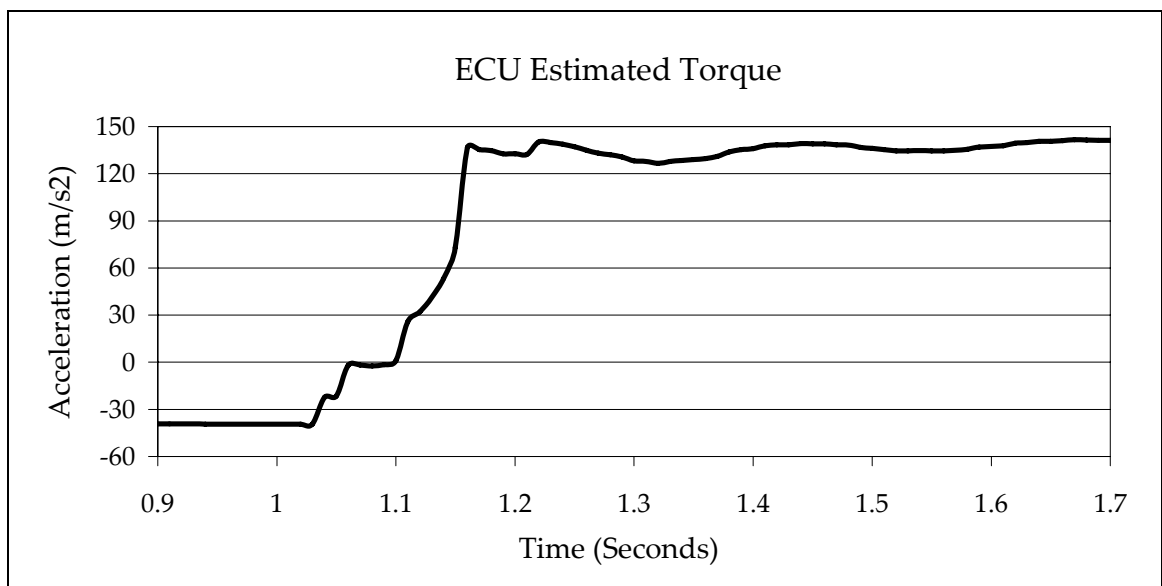


Figure 5.4.2: ECU Estimated Engine Torque Data

Figure 5.4.3 compares the filtered accelerometer data and modelled acceleration response for a ramp in engine torque from -40 Nm to 130 Nm in 0.15 seconds. From Figure 5.4.3 it is clear that the complex model accurately predicts the shunt and shuffle in the drivetrain, and it can therefore be concluded that this model is an accurate vehicle simulation tool.

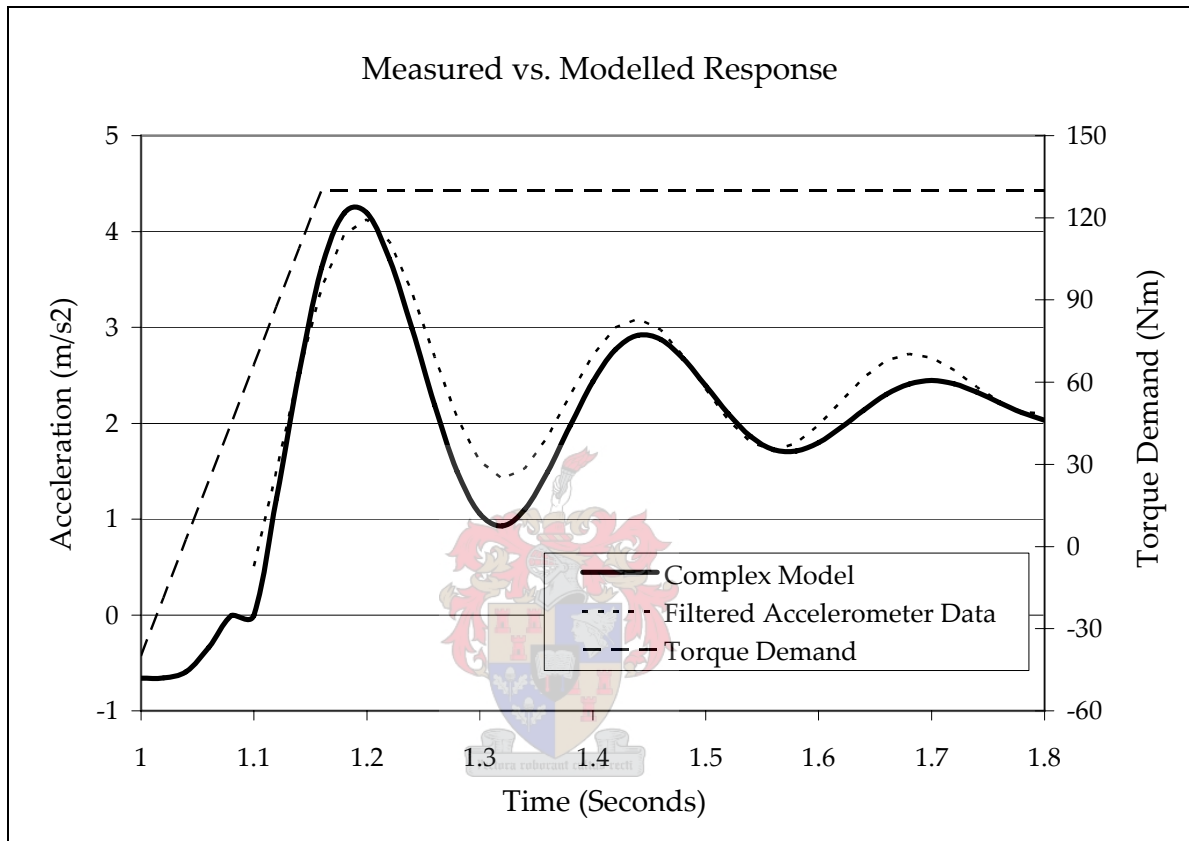


Figure 5.4.3: Measured vs. Modelled Response (-40 Nm to 130 Nm in 0.15 seconds)

# Controller Development

---

# 6

## 6.1 Introduction

In an effort to improve driveability, a basic slew-rate limiter could be used to limit the rate of change of engine torque. Although this would soften the high frequency content of the drivetrain response, better results could be obtained using a feedback control system. A drivetrain controller, including a state estimator, was therefore designed. The primary objective of the controller was to reduce the shunt and shuffle in the drivetrain without reducing the vehicle's responsiveness to a torque demand. Otherwise stated, the input torque signal had to be controlled so as to ensure the desirable acceleration of the vehicle. As explained in Chapter 5, the vehicle's shunt and shuffle is worst in first gear, and the controller was therefore designed for this gear.

## 6.2 Control Strategy

A simple robust linear controller was required, and personal comments by Treurnicht (2005) led to the derivation presented in this section. The simplified model derived in Section 3.3 resulted in a second-order transfer function relating engine torque to driveshaft torque. For this reason, second-order dynamics were considered when devising a control strategy.

The transfer function of a second-order system is:

$$\frac{y(s)}{u(s)} = \frac{\omega_n^2}{s^2 + 2 \cdot \zeta \cdot \omega_n \cdot s + \omega_n^2} \quad (6.2.1)$$

The system input is  $u$  and the output is  $y$ . The damping ratio of the system is  $\zeta$  and the natural (dominant) frequency is  $\omega_n$ . Converting (6.2.1) from the s-plane into the time domain gives:

$$y(t) = u(t) - \left(\frac{1}{\omega_n^2}\right) \cdot \ddot{y} - \left(\frac{2\zeta}{\omega_n}\right) \cdot \dot{y} \quad (6.2.2)$$

The ideal controller must increase the damping of the system, thereby reducing the overshoot and oscillations in the step response. From (6.2.2) it is clear that only the term with the derivative of the output  $y$  has an effect on the damping of the system. The obvious solution to the problem was to therefore increase the damping term by using the negative feedback of this derivative. If this feedback had a gain  $K$ , the second order dynamics would become:

$$y(t) = u(t) - \left(\frac{1}{\omega_n^2}\right) \cdot \ddot{y} - \left(\frac{2\zeta}{\omega_n} + K\right) \cdot \dot{y} \quad (6.2.3)$$

The system's damping has therefore been increased, and the new damping ratio is:

$$\zeta_{new} = \left(\zeta + \frac{K \cdot \omega_n}{2}\right)$$

If the torque demand in the vehicle is the input  $u(t)$ , the wheel torque is the system output  $y(t)$ . Because the vehicle's acceleration is directly proportional to the wheel torque, it can also be used as the system output  $y(t)$ , and the control strategy can use the derivative of either of these signals to construct the final control signal. Due to the fact that these derivatives are not measurable, an estimator must be used to calculate one of them. A block diagram of the control strategy is shown in Figure 6.2.1.

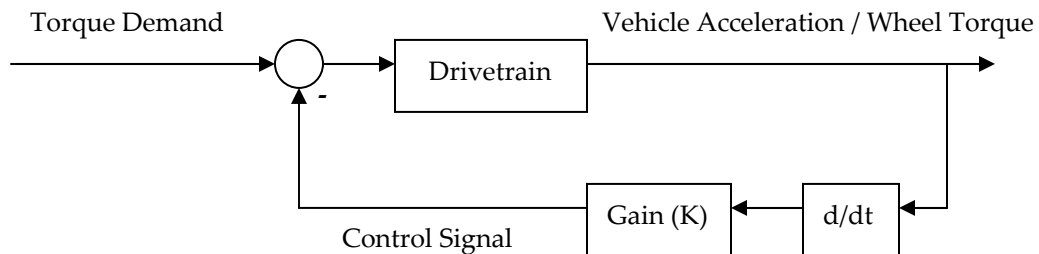


Figure 6.2.1: Control Strategy

## 6.3 Estimator Design

### 6.3.1 Estimator Theory

The behaviour of a system is often described by writing a state-space description of the form:

$$\dot{x} = Ax + Bu \quad (6.3.1)$$

$$y = Cx \quad (6.3.2)$$

$A$ ,  $B$  and  $C$  are the system matrices and  $x$ ,  $y$  and  $u$  are the state, output and input vectors respectively. The measured outputs of the system are given by (6.3.2) and are a combination of the state variables found in vector  $x$ .

It is often not possible to measure all of the state variables. This is due to the fact that sensors that are capable of measuring certain system states are too expensive, or the measurement signals obtained are simply too noisy. If this is the case, a mathematical model of the system can be used along with the available state measurements ( $y$ ) to derive an estimate of the unknown states. This process is known as state estimation and the estimator equations are:

$$\dot{\hat{x}} = A\hat{x} + Bu + L(y - \hat{y}) \quad (6.3.3)$$

$$\hat{y} = C\hat{x} \quad (6.3.4)$$

The estimated output and state vectors are  $\hat{y}$  and  $\hat{x}$  respectively.  $L$  is known as the estimator gain matrix, and if it is chosen carefully it can ensure that the estimated states track the actual states closely.

### 6.3.2 Drivetrain Estimator

The third-order linear drivetrain model derived in Chapter 3 was used to construct the state estimator. The resulting system matrices were:

$$A = \begin{bmatrix} 0 & -1 & \frac{1}{it} \\ \frac{k_s}{I_c} & -\frac{c_s}{I_c} & \frac{c_s}{it \cdot I_c} \\ -\frac{k_s}{it \cdot I_f} & \frac{c_s}{it \cdot I_f} & \frac{-c_s}{it^2 \cdot I_f} \end{bmatrix} \quad (6.3.5)$$

$$B = \begin{bmatrix} 0 & 0 \\ 0 & -\frac{1}{I_c} \\ \frac{1}{I_f} & 0 \end{bmatrix} \quad (6.3.6)$$

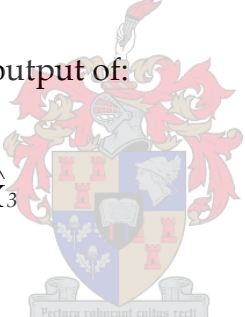
The state vector ( $x$ ) was:

$$\begin{bmatrix} X_1 \\ X_2 \\ X_3 \end{bmatrix} = \begin{bmatrix} \left(\frac{\theta_f}{i_t} - \theta_w\right) \\ \dot{\theta}_w \\ \dot{\theta}_f \end{bmatrix} \quad (6.3.7)$$

The wheel and engine speed ( $X_2$  and  $X_3$ ) are both measured in the vehicle. Because the resolution of the wheel speed measurement is far lower than that of the engine speed measurement, it was decided to use the engine speed as the measurement signal to the estimator. The resulting C matrix was therefore:

$$C = [0 \quad 0 \quad 1] \quad (6.3.8)$$

This resulted in an estimated output of:

$$\hat{y} = [0 \quad 0 \quad 1] \begin{bmatrix} \hat{X}_1 \\ \hat{X}_2 \\ \hat{X}_3 \end{bmatrix} = \hat{X}_3 \quad (6.3.9)$$


Since the driveshaft is the dominant element in the drivetrain, if the load on the wheel ( $T_L$ ) is treated as a disturbance it can be assumed that the torsion in the driveshaft is approximately equal to the wheel torque. The derivative of this torsion can therefore be used to construct the control signal. The driveshaft torsion is a state in the system model:

$$X_1 = \left(\frac{\theta_f}{i_t} - \theta_w\right) \quad (6.3.10)$$

The derivative of this torsion can be obtained by combining states  $X_2$  and  $X_3$ :

$$\dot{X}_1 = \left(\frac{\dot{\theta}_f}{i_t} - \dot{\theta}_w\right) = \left(\frac{X_3}{i_t} - X_2\right) \quad (6.3.11)$$

This combination of states can now be multiplied by gain  $K$  and used as the feedback control signal.



### 6.3.3 Estimator Gains

Kalman filter gains (Franklin et. al., 1998) were used in the estimator. In calculating these gains, the process noise co-variance ( $R_w$ ) and measurement noise co-variance ( $R_v$ ) were first calculated.

A higher process noise implies modelling inaccuracies and forces the estimator to weigh the measured values more highly than the modelled values when calculating the estimated states. Alternatively, a higher measurement noise implies that the measurement signal is more inaccurate than the model and forces the estimator to rely on the modelled state values more than on the measured values. The approach used to determine the noise co-variances was to first calculate the typical measurement noise RMS value, and to then calculate the resulting measurement noise co-variance using  $R_v = RMS^2$ . The process noise co-variance was then determined by trial and error until the resulting estimator gains ensured that the estimated states tracked the actual states accurately, with minimal noise present in the estimated signals.

In Momberg (2005), a 1.6 litre Volkswagen Jetta was driven at constant speeds and the engine speed was recorded by the ECU. The speed variation (noise) from this signal is shown in Figure 6.3.1. The noise was assumed to be white (uncorrelated) with a zero mean and its RMS value was calculated as  $0.524 \text{ rad}\cdot\text{s}^{-1}$ . The measurement noise co-variance ( $R_v$ ) was therefore  $0.275 \text{ rad}^2\cdot\text{s}^{-2}$ . A process noise covariance of  $R_w = 110$  was chosen.

Since the engine speed was sampled by the ECU every 0.01 seconds, this sample time was also chosen for the controller. The estimator matrices were discretized (Appendix D) and the resulting estimator gains were calculated in Matlab using the 'Kalman' function:

$$L = \begin{bmatrix} 0 \\ 0.0011 \\ 0.0167 \end{bmatrix} \quad (6.3.12)$$

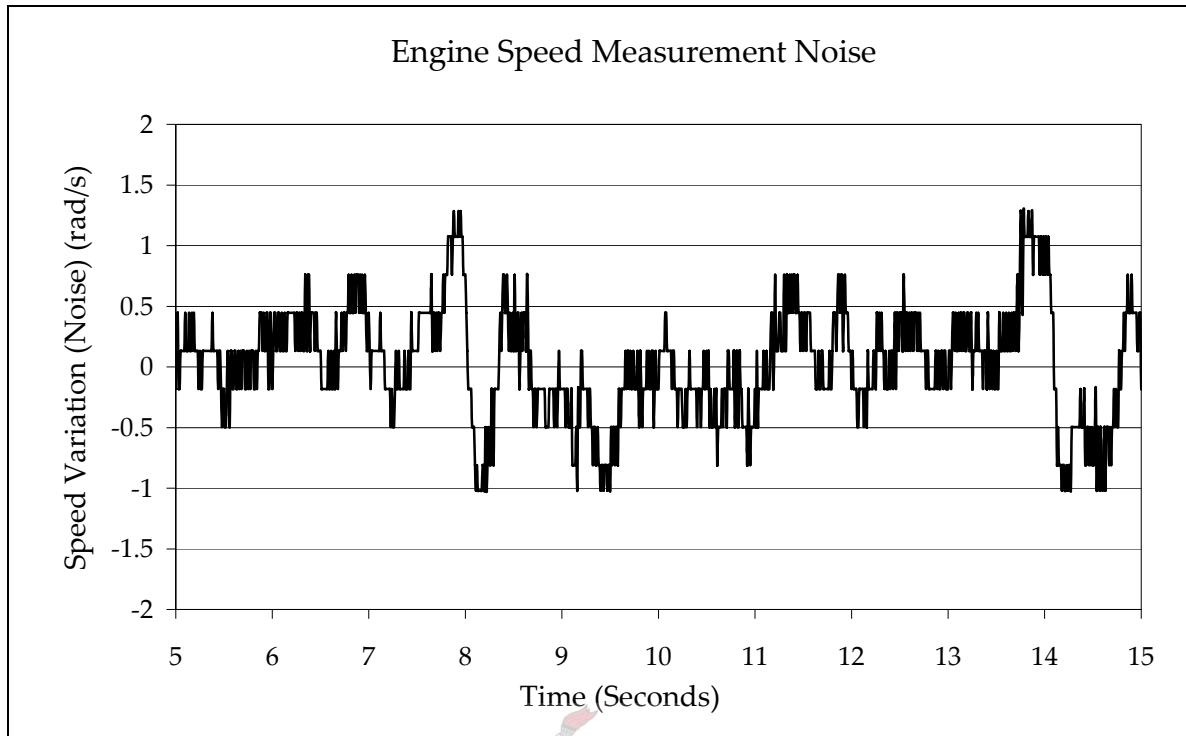


Figure 6.3.1: Engine Speed Measurement Data Noise

### 6.3.4 Estimator Performance

The estimator performance will now be analyzed for the uncontrolled system. The estimated and modelled engine and wheel speeds for the system are compared for the scenario when the drivetrain does not pass through the backlash region. Figure 6.3.2 and Figure 6.3.3 show that the estimated values track the actual (modelled) values well. This was expected as the third-order drivetrain model used in the estimator simulates the actual vehicle behaviour well when the backlash region is avoided. It is clear that the modelled engine speed lags slightly behind the estimated value. This is due to the fact that the simplified model used in the estimator does not account for the engine's transport delay.

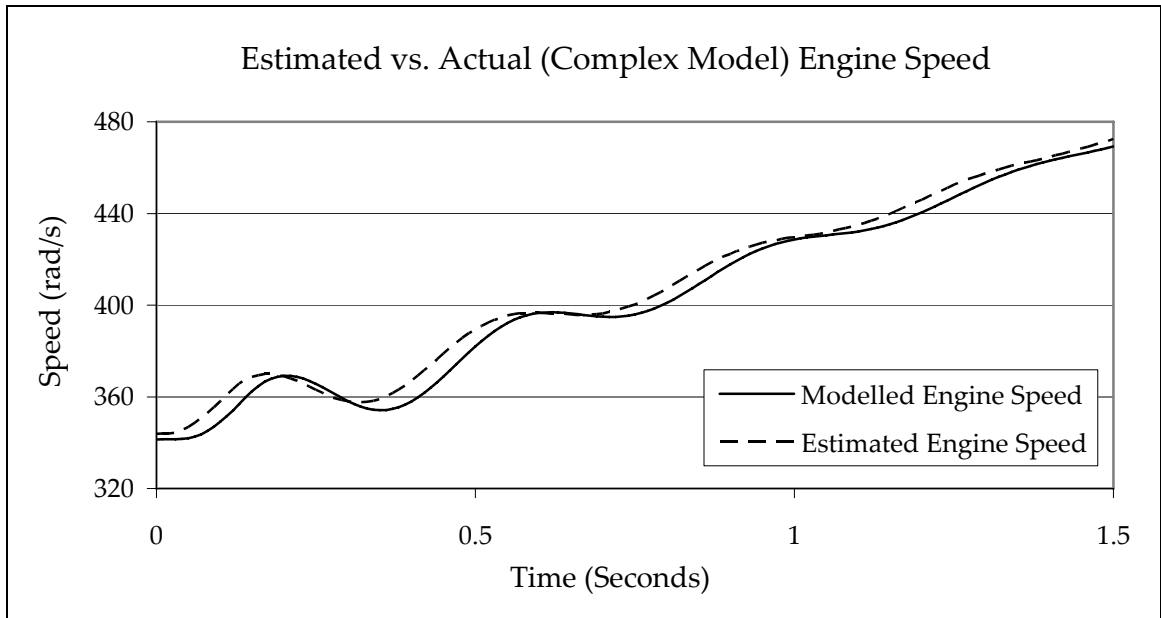


Figure 6.3.2: Estimated vs. Actual (Complex Model) Engine Speed (No Backlash)

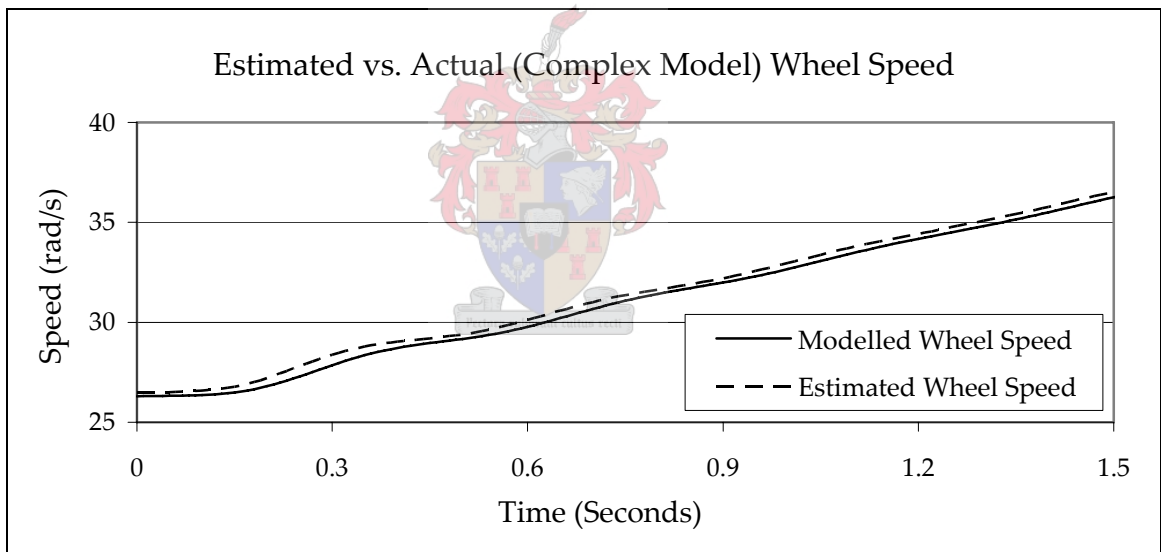


Figure 6.3.3: Estimated vs. Actual (Complex Model) Wheel Speed (No Backlash)

Figure 6.3.4 compares the modelled and estimated engine speeds when the drivetrain passes through the backlash region, and Figure 6.3.5 compares the modelled and estimated wheel speeds. It is clear that the estimator doesn't track the speeds quite as well as before although the results are still acceptable. This slightly inaccurate estimation was expected as the linear model used in the estimator did not account for backlash. The estimator could be extended to include the non-linearity; however it is shown in Chapter 7 that the linear model's performance was sufficient to achieve good drivetrain control.

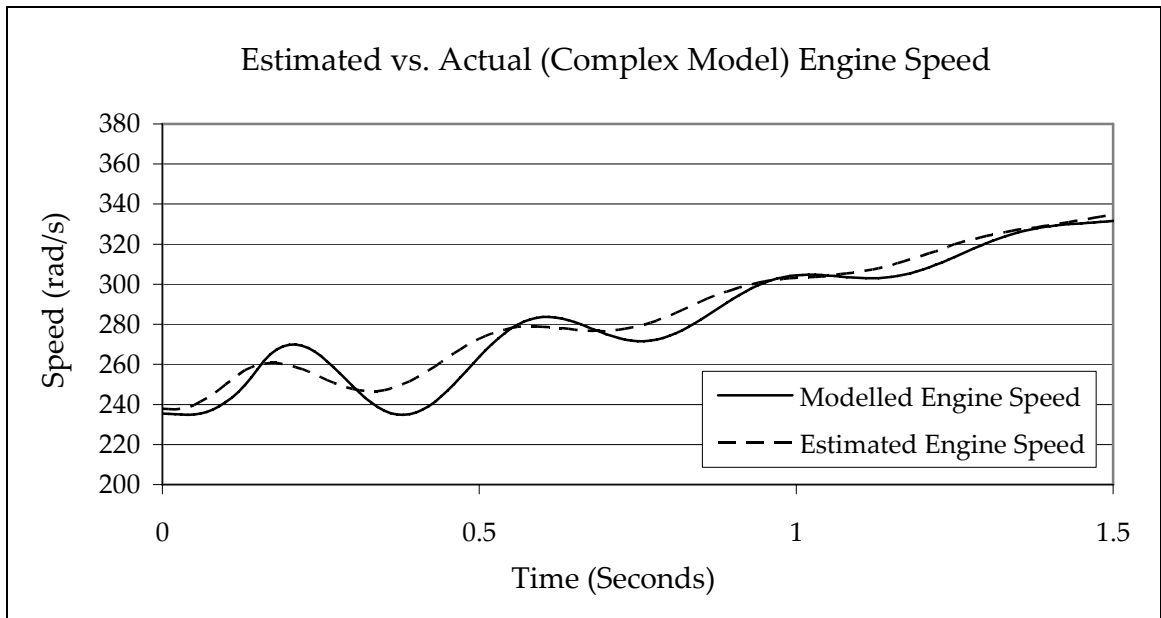


Figure 6.3.4: Estimated vs. Actual (Complex Model) Engine Speed (Backlash)

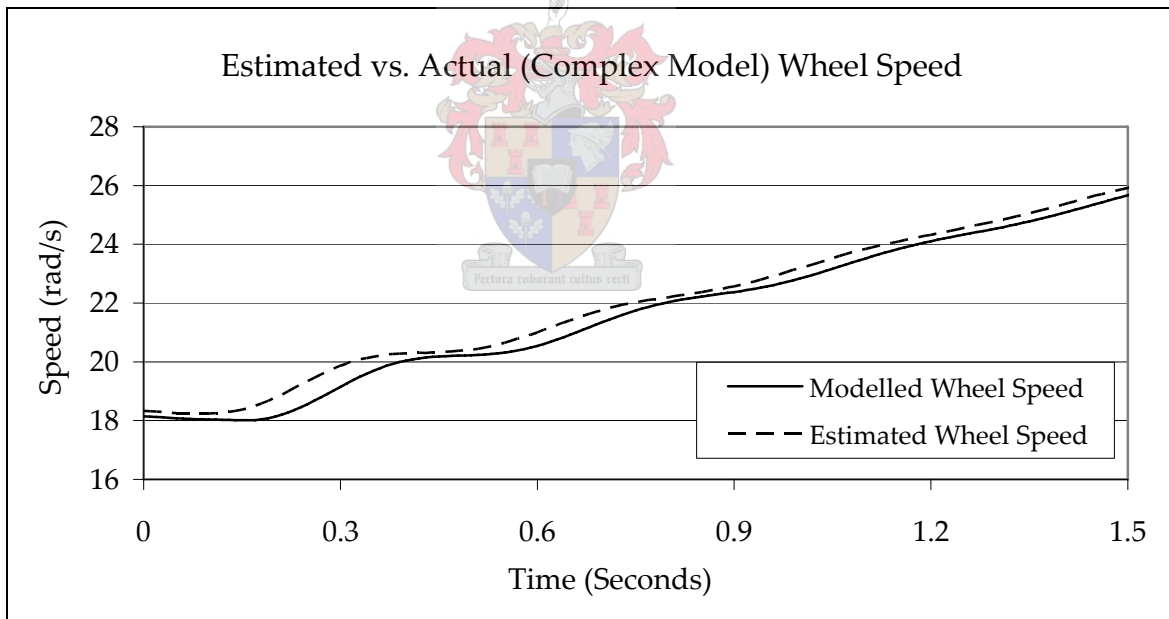


Figure 6.3.5: Estimated vs. Actual (Complex Model) Wheel Speed (Backlash)

The engine speed sensor signal is noisy and, as previously stated, the estimator's role is to use this signal to produce a 'filtered' engine speed estimate. For a final indication of the estimator's performance, Figure 6.3.6 compares the estimated engine speed (estimator output) and the modelled engine speed with sensor noise (estimator input). It is clear that the estimator filters the signal well.

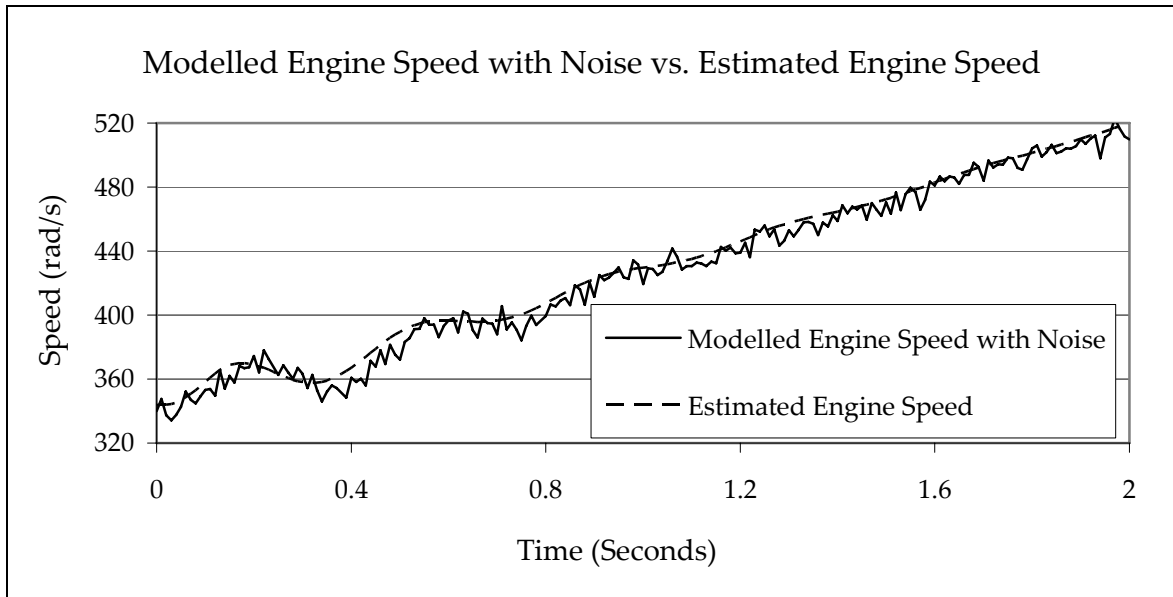


Figure 6.3.6: Modelled Engine Speed with Noise vs. Estimated Engine Speed

## 6.4 Control System

A schematic overview of the control system is shown in Figure 6.4.1. The estimator is used to estimate the engine and wheel speeds from the measured engine speed and torque demand signals. These speed estimates are then combined to calculate the rate of change of drivetrain torsion. This signal in turn is multiplied by a gain and subtracted from the driver's torque demand input signal to the engine.

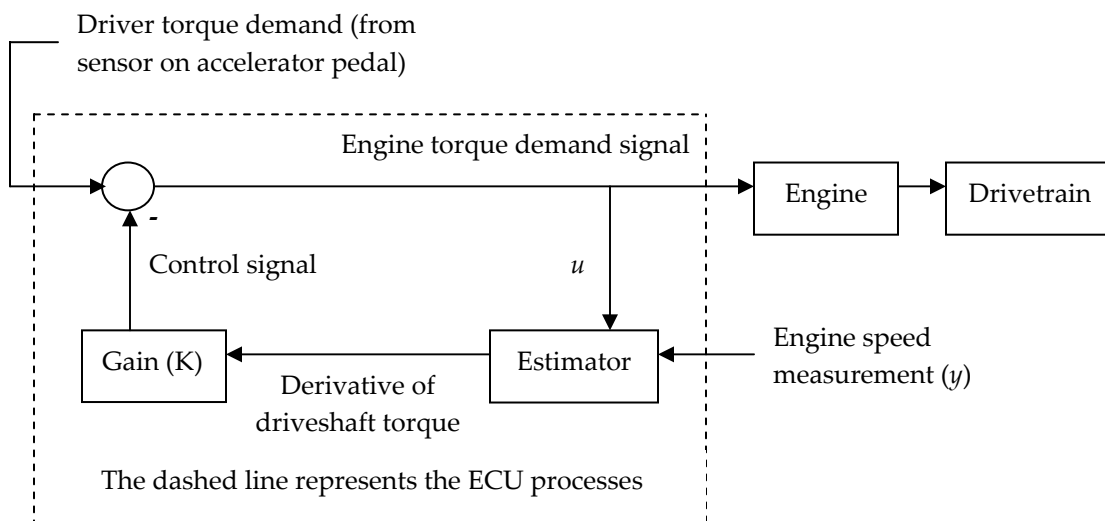


Figure 6.4.1: Schematic Overview of the Control System

---

# Controller Performance

---

# 7

## 7.1 Introduction

This chapter evaluates the performance of the control system. First, the effect of various control gains on the acceleration response of the drivetrain is investigated. Final control gains are then chosen and the controller's performance is analysed. To put the controller's performance into perspective, it is compared to the performance of a basic torque rate limiter which limits the rate of change of driver torque demand. Finally, possible improvements to the controller are investigated.

## 7.2 Control Gains

The controller's performance was analyzed for various control gains ( $K$ ). This was done using the complex drivetrain model in Matlab / Simulink to simulate the vehicle's behaviour with the controller code implemented. Figure 7.2.1 shows the vehicle's acceleration response for various control gains when the backlash region is avoided. As in Chapter 5, a torque ramp input from 10 Nm to 90 Nm in 0.1 seconds was used to simulate this scenario. It is clear that the faster the response, the larger the overshoot.

Figure 7.2.2 plots the total integrated error as well as the percentage overshoot error in the response for various control gains. The total integrated error was calculated as the area between the acceleration response curve and the acceleration demand curve. This value was converted into a percentage by dividing it by the

area under the acceleration demand curve. It is clear that a gain of 60 results in zero overshoot, while a gain of 40 results in the minimum total integrated error.

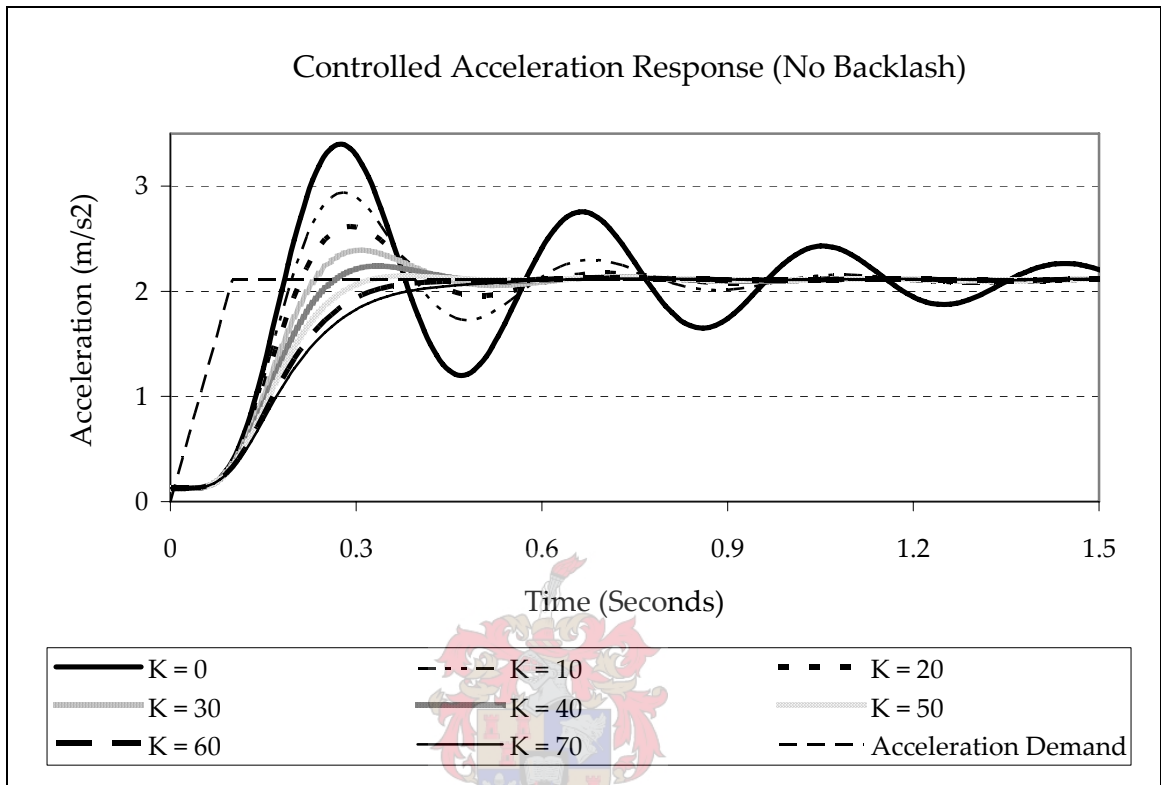


Figure 7.2.1: Controlled Acceleration Response (No Backlash)

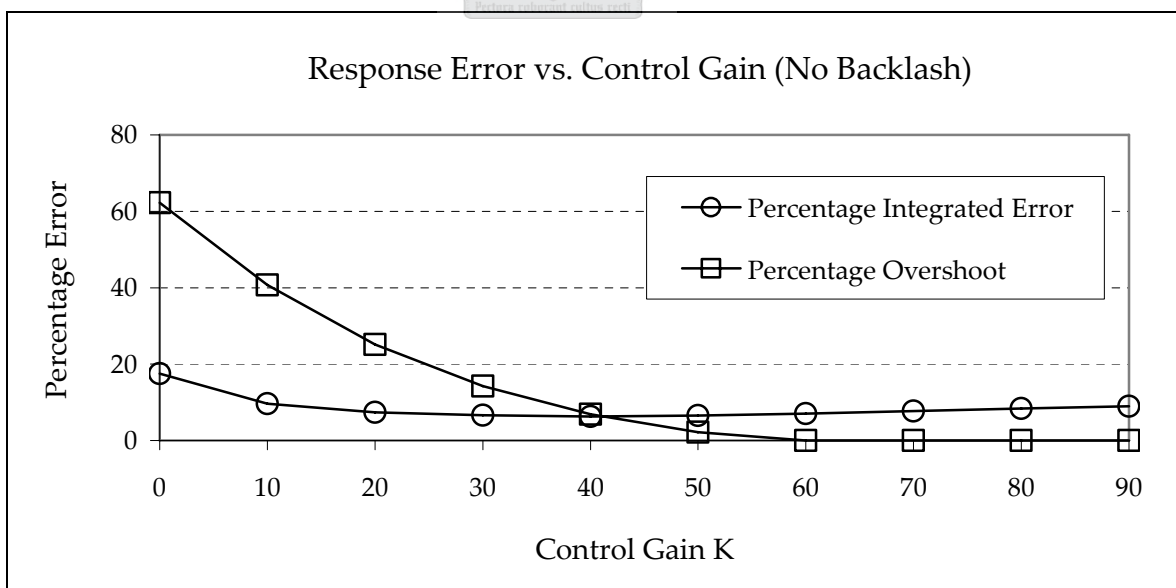


Figure 7.2.2: Response Error vs. Control Gain (No Backlash)

Figure 7.2.3 shows the acceleration responses for various gains when the drivetrain passes through the backlash region. As in Chapter 5, a torque ramp input from -10 Nm to 70 Nm in 0.1 seconds is used to simulate this scenario. It is clear that the controller does not perform as well for this scenario as it did for the scenario when the backlash region was avoided. This will be discussed in further detail in Section 7.3.

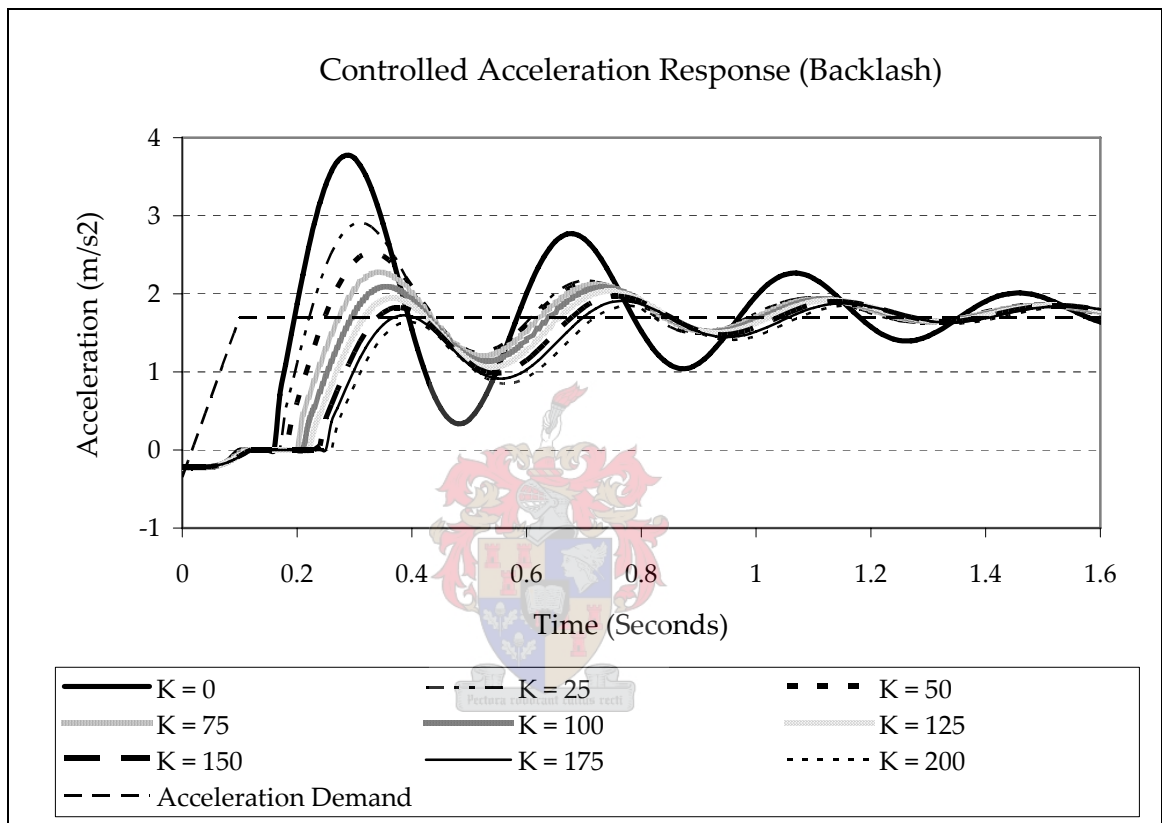


Figure 7.2.3: Controlled Acceleration Response (Backlash)

Figure 7.2.4 shows the error in the response for various control gains when the drivetrain passes through the backlash region. A gain of 150 results in zero overshoot while a gain of 75 results in the minimum total integrated error. It is clear that for optimal performance, higher gains are required for this scenario than for when the backlash region is avoided.



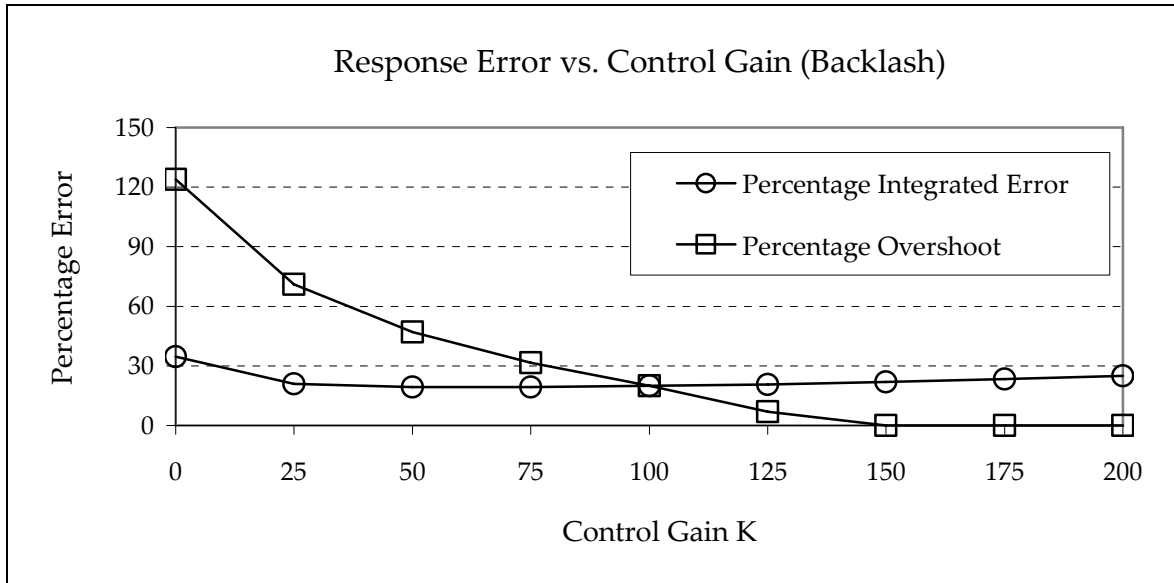


Figure 7.2.3: Response Error vs. Control Gain (Backlash)

Figure 5.4.2 is an example of a data set from the torque estimation algorithms in the ECU. As described earlier, the backlash region can be identified as the period for which the torque is approximately zero. This available torque estimate can be used to switch between control strategies depending on whether the drivetrain is close to the backlash region or not. For example; if the engine torque is negative, a control gain best suited to the backlash scenario can be used, or if the engine torque is positive, a control gain best suited to the scenario where the backlash region is avoided can be implemented. Final control gains of 50 and 100 were decided on for the backlash and no backlash scenarios respectively.

## 7.3 Controller Performance Analysis

The final controller is now analyzed in more detail. Figure 7.3.1 gives a clear indication of the performance of the controller when the backlash region is avoided ( $K = 50$ ).

The rise time is defined as the time taken for the system to go from 10% to 90% of its steady-state value. The settling time is defined as the time taken for the system to settle to within 99% of its steady-state value. The controlled response has a rise time of 0.19 seconds, a settling time of 0.65 seconds and an overshoot of 2.2%. The uncontrolled response has a rise time of 0.1 seconds, but it has a settling time of 1.31 seconds and an overshoot of 62.2%. As shown in Figure 7.2.2, with the

controller gain of 50 the total integrated error in the response has been reduced by 11.0%. The controller has therefore significantly reduced the shunt and shuffle.

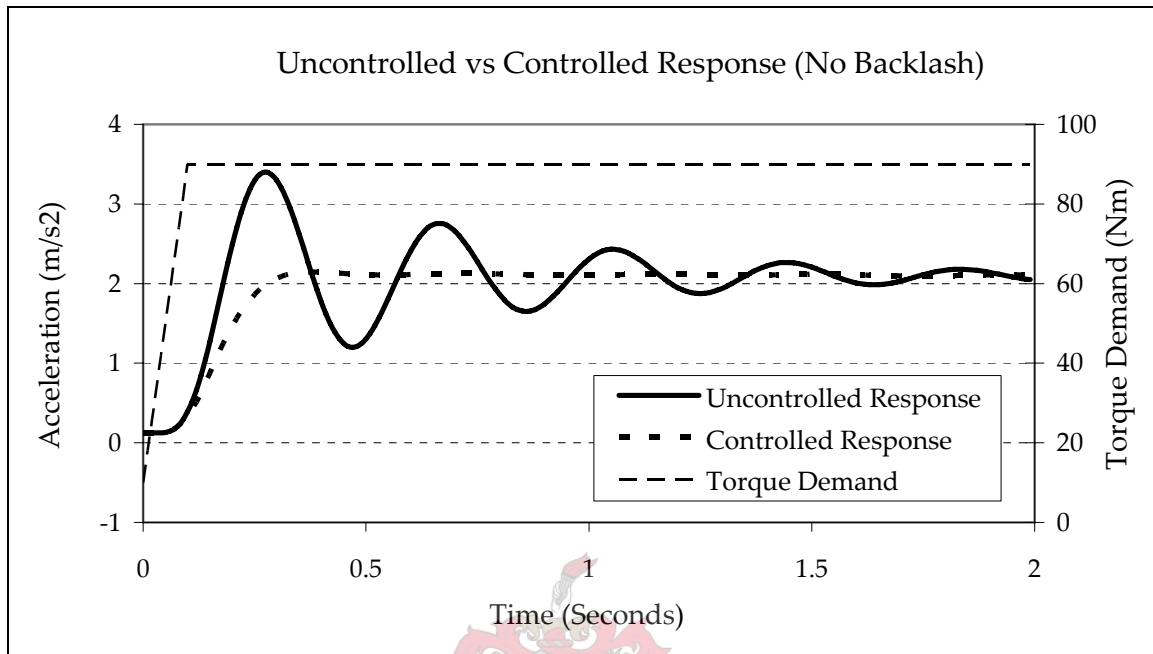


Figure 7.3.1: Uncontrolled vs. Controlled Response (No Backlash)

Figure 7.3.2 compares the controlled and uncontrolled responses when the drivetrain passes through the backlash region. Although the system behaviour is improved significantly, the controller does not result in as smooth a response as it did for the scenario when the backlash region was avoided. This is primarily due to two factors. Firstly, the estimator did not account for the backlash non-linearity in its system model, and therefore did not track the system states very accurately through this region. Secondly, there is a large instantaneous torque impact in the drivetrain as it exits the backlash region. This results in a system that is a lot harsher than when the backlash region was avoided. The effect of this large impact is clearly indicated by the fact that the uncontrolled system now has an overshoot of 123.9% as opposed to the 62.2% overshoot when it did not pass through the backlash region.

The controlled response (with  $K = 100$ ) has a rise time of 0.17 seconds, a settling time of 1.6 seconds and an overshoot of 19.9%. As with the scenario when the backlash region was avoided this is a big improvement, as the uncontrolled response had a rise time of 0.10 seconds, a settling time of 1.9 seconds and an overshoot of 123.9%. The controller reduced the total integrated error by 14.7%.

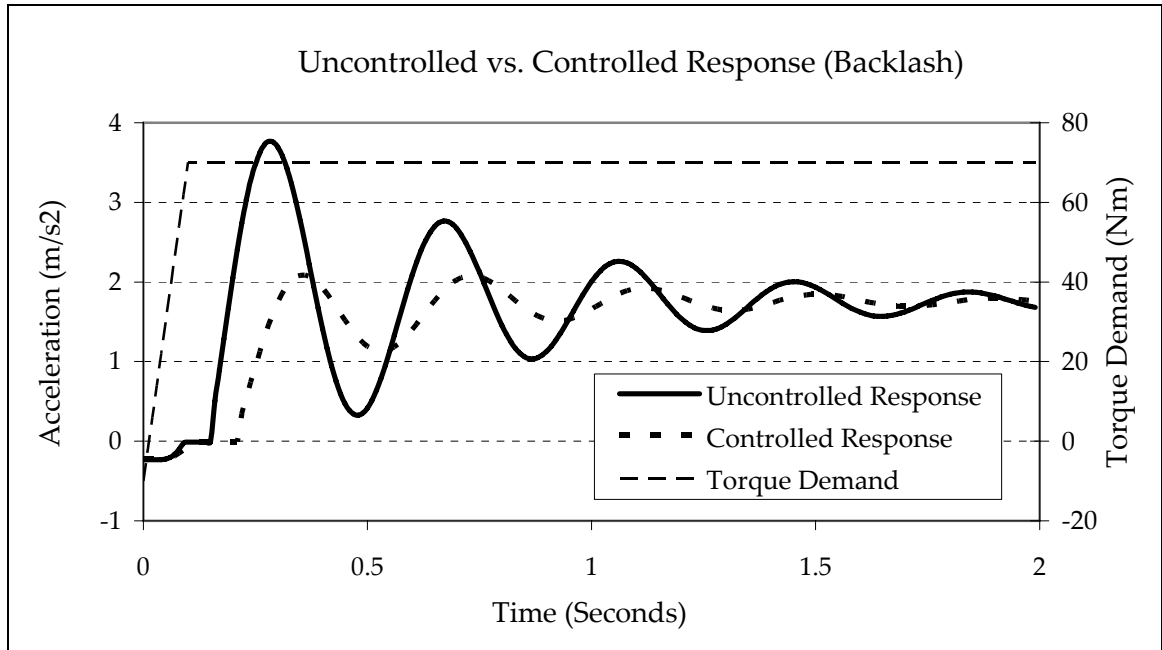


Figure 7.3.2: Uncontrolled vs. Controlled Response (Backlash)

Figure 7.3.3 illustrates the engine speed increase for both the uncontrolled and controlled systems. The torque demand was a ramp input from 10 Nm to 90 Nm in 0.1 seconds. It is clear that the amplitude of the oscillations in engine speed has also been reduced significantly.

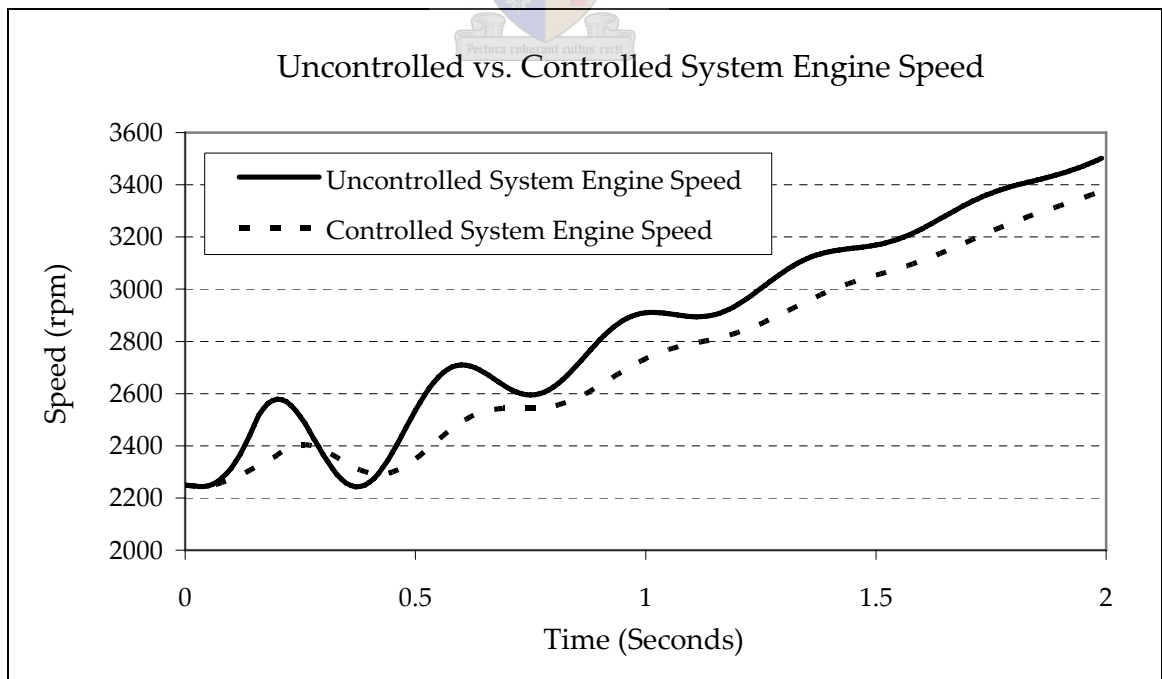


Figure 7.3.3: Uncontrolled vs. Controlled Engine Speed

The driver's torque demand and the controlled (adjusted) engine torque demand signal are shown in Figure 7.3.4. In this thesis the assumption was made that the throttle plate responded instantaneously to a given demand. In reality this is not the case, and certain throttle body delays and dynamics exist that can limit the rate of change of torque. These delays and dynamics are of consequence when sharp torque changes like the one shown in the control signal in Figure 7.3.4 are required. By varying the ignition timing and air-fuel ratios, torque changes of small amplitude can be achieved in far less time than by changing the throttle body position. Part of the ECU's engine torque management strategy is to analyse the torque demand signal and to ensure that it is followed as closely as possible using any one of the above mentioned methods. In the current study it was assumed that the ECU ensured that the engine torque followed the demand signal perfectly.

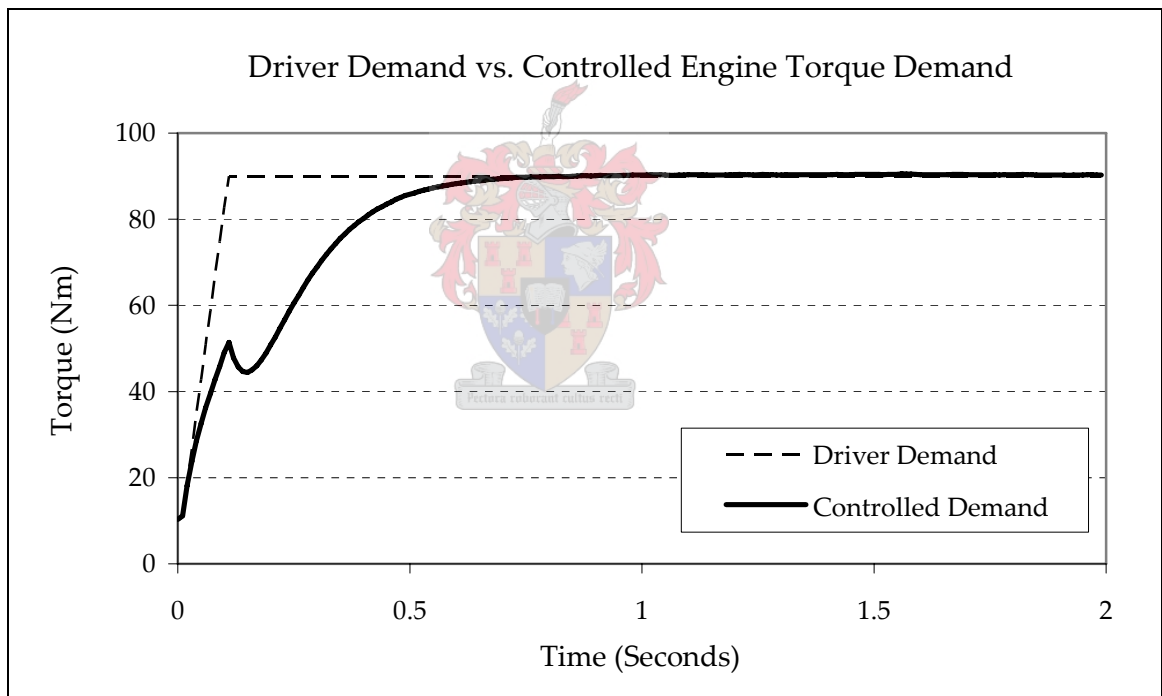


Figure 7.3.4: Driver Demand vs. Controlled Engine Torque Demand

In summary it has been shown that the controller will significantly reduce the shunt and shuffle in the vehicle for both scenarios without reducing the vehicle's responsiveness to a torque demand.

## 7.4 Comparison with a Torque Rate Limiter

In order to put the performance of the controller into perspective, it was compared to the performance of a basic torque rate limiter. The rate limiter was applied to the driver's torque demand signal and it limited the rate of change of torque so as to ensure that shunt and shuffle were not induced in the drivetrain.

Figure 7.4.1 compares the two strategies for the scenario when the backlash region is avoided. A torque input ramp from 10 Nm to 90 Nm in 0.1 seconds was once again used. The controller resulted in a rise time of 0.19 seconds, a settling time of 0.65 seconds and an overshoot of 2.2%, while the torque rate limiter resulted in an overshoot of 6.9%, a rise time of 0.25 seconds and a settling time of 1.35 seconds. It is therefore clear that the controller out-performs the rate limiter.

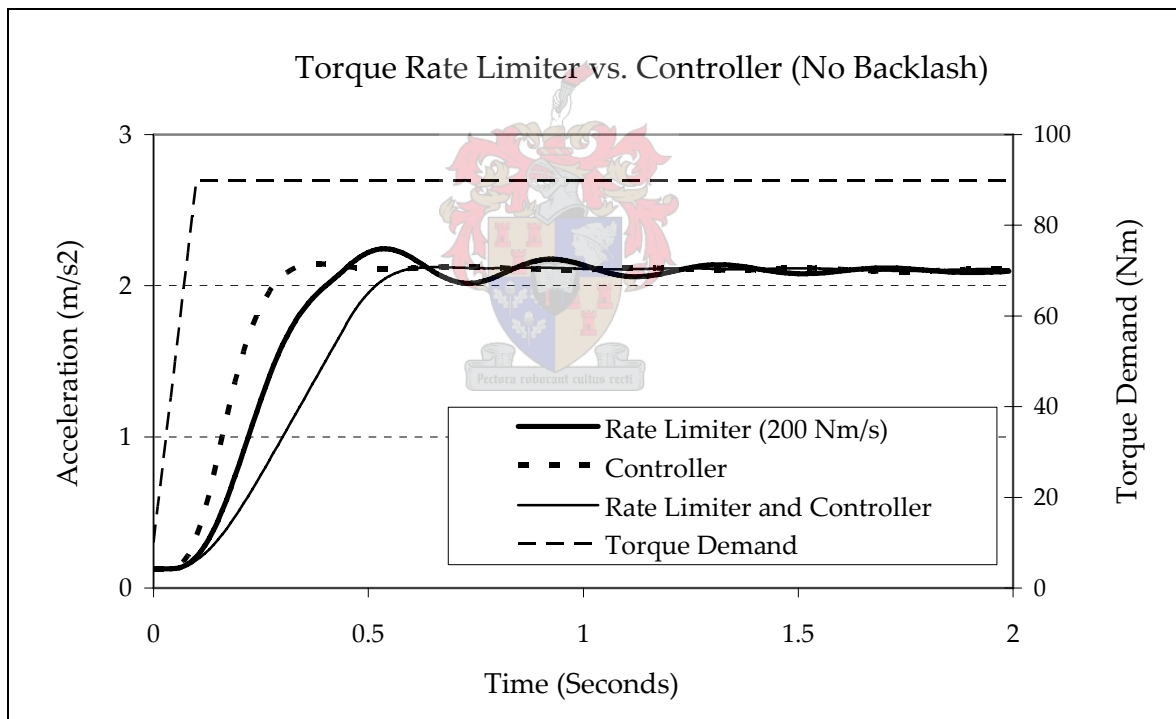


Figure 7.4.1: Torque Rate Limiter vs. Controller (No Backlash)

Figure 7.4.2 compares the two strategies for the scenario when the drivetrain passes through the backlash region. A torque ramp from -10 Nm to 70 Nm in 0.1 seconds was used as the input. The controller results in a rise time of 0.17 seconds, a settling time of 1.6 seconds and an overshoot of 19.9%, while the rate limiter results in the same overshoot and settling time but a rise time which is 0.05 seconds slower.

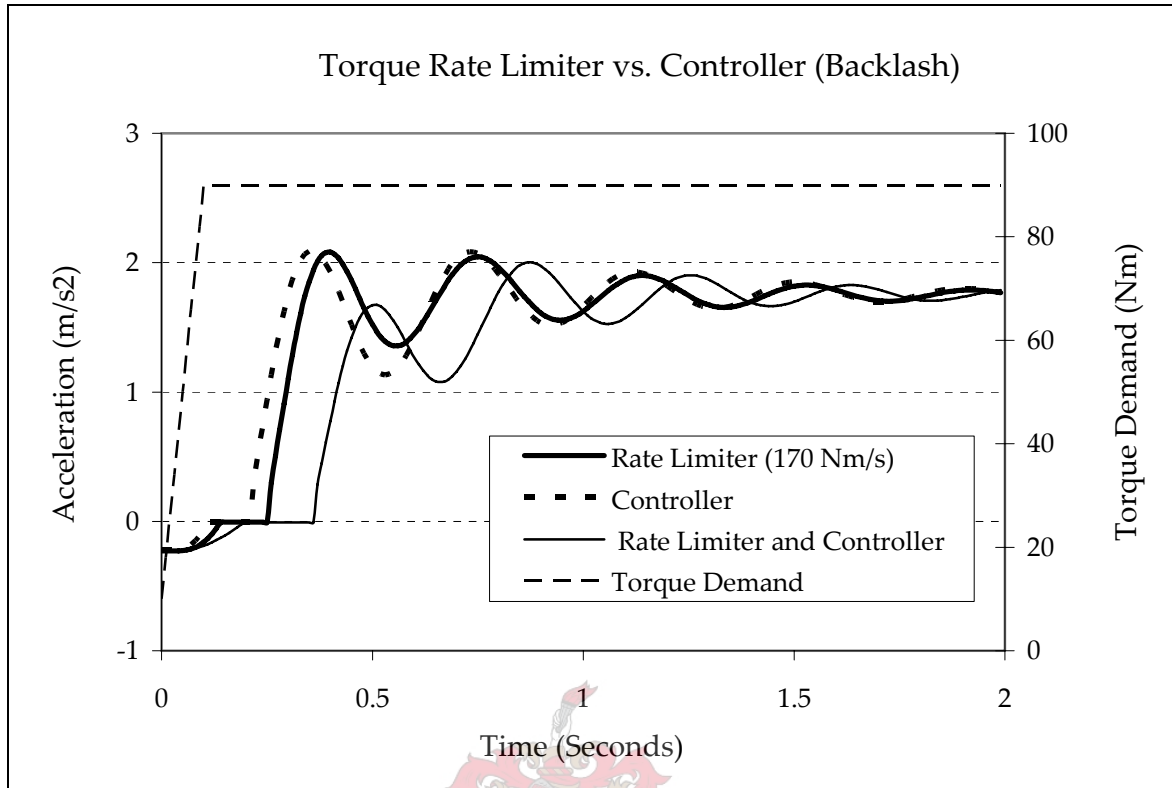


Figure 7.4.2: Torque Rate Limiter vs. Controller (Backlash)

Although the performance of the controller is superior to that of the rate limiter in both scenarios, the rate limiter's performance is surprisingly good for a system that is far less complex than the controller. Combining the rate limiter and controller results in a much slower rise time than for either of the individual systems.

## 7.5 Possible Improvements

The control strategy used in this thesis was based on increasing the damping of the drivetrain. This strategy worked well when the system behaved linearly and the backlash region was avoided, however when the backlash region was not avoided the performance of the controller (although still good) deteriorated. To achieve improved results the engine torque would have to be actively controlled as the drivetrain passes through the backlash region. This strategy would require accurate knowledge of when the drivetrain is in the backlash region. Lagerberg et. al. (2002) investigated this strategy and concluded that slightly inaccurate backlash estimation could result in instability issues. Robustness in the drivetrain is essential and this approach was therefore not given further consideration in the current study.

# Conclusion

---

# 8

This thesis consisted of several stages, all of which were successfully completed. Initially a comprehensive literature study was carried out. The results were helpful in determining what research had already been done in the field of drivetrain modelling and control, and how best to approach the current study.

Next, two different mathematical models of the drivetrain were derived. One was a complex non-linear model which accounted for the backlash in the drivetrain, and the other was a simplified linear model which did not account for the backlash.

An experimental test bed was then designed, manufactured and assembled so that the drivetrain could be driven by a large DC motor. Since the speed and torque of the DC motor could be accurately controlled, this setup provided a simple means of characterising the various drivetrain components. Various sensors were mounted to the test-rig, and data acquisition software was written for each of them. The experimentation resulted in parameter values being obtained for the majority of the drivetrain components, and the remaining component parameter values were obtained using vehicle measurement data and references.

The component parameter values obtained through experimentation were then used in the mathematical models of the drivetrain, and simulations were performed that predicted the response of the vehicle to various driver torque demands. The following two conclusions were drawn from these simulations:

1. The driveshaft is the dominant contributor to drivetrain dynamics in low gears.
2. The clutch dynamics have no effect on the dominant drivetrain frequency in low gears.

Test data obtained through vehicle testing was used to confirm the accuracy of the simulations. It was found that the complex model predicted the actual vehicle behaviour accurately, and it was concluded that the model was a useful vehicle simulation tool.

Next, a robust linear controller and estimator were designed to reduce the shunt and shuffle in the drivetrain. The effect of various control gains on the response was analyzed using the vehicle model, and final control gains were chosen so as to achieve the optimum trade-off between vehicle response time and driveability. Finally, simulations were performed to predict the performance of the controller. It was concluded that the controller reduced the shunt and shuffle in the vehicle significantly while still maintaining fast vehicle response times. A recommendation for future work would therefore be the implementation and calibration of the controller in the ECU of a vehicle.

In conclusion, it is clear that the objectives of this thesis as described in Chapter 1 were all successfully achieved, and it has been shown that a vehicle drivetrain can be modelled, simplified, estimated and controlled to improve vehicle driveability.



---

# References

C. Canudas-De-Wit, P. Tsiotras, E. Velenis, M. Basset, G. Gissinger, 2003, *Dynamic Friction Models for Road / Tyre Longitudinal Interaction*, *Vehicle System Dynamics*, Volume 39, Number 3.

P. A. Conradie, 2001, *The Development of a Dynamic Engine-Testing Facility*, Masters Thesis, Department of Mechanical Engineering, University of Stellenbosch, Stellenbosch, South Africa.

G. F. Franklin, J. D. Powell, M. Workman, 1998, *Digital Control of Dynamic Systems*, 3<sup>rd</sup> Edition, Addison Wesley Longman, CA, U.S.A.

G. F. Franklin, J. D. Powell, A. Emami-Naeini, 2002, *Feedback Control of Dynamic Systems*, 4<sup>th</sup> Edition, Prentice Hall, New Jersey, U.S.A.

J. Fredriksson, 1999, *Non-Linear Control of Turbocharged Diesel Engines – An Integrated Powertrain Control Perspective*, Licentiate Thesis, Technical Report 329L, Department of Signals and Systems, Chalmers University of Technology, Göteborg, Sweden.

J. Fredriksson, H Weiefors, B.S. Egardt, 2002, *Powertrain Control for Active Damping of Driveline Oscillations*, *Vehicle System Dynamics*, Taylor and Francis, Volume 37, Number 5.

R. C. Hibbeler, 1997, *Engineering Mechanics - Dynamics*, 7<sup>th</sup> Edition, Prentice Hall, Singapore.

S. Johansson, 2004, *Shunt and Shuffle Evaluation for Vehicle Powertrains*, Masters Thesis, Mechanical Engineering Department, Chalmers University of Technology, Göteborg, Sweden.

J. Karlsson, 2001, *Powertrain Modeling and Control for Driveability in Rapid Transients*, Thesis for the degree of Licentiate of Engineering, Department of Machine and Vehicle Design, Chalmers University of Technology, Göteborg, Sweden.

A. Lagerberg, 2001, *A Literature Survey on Control of Automotive Powertrains with Backlash*, Report R013/2001, Department of Signals and Systems, Chalmers University of Technology, Göteborg, Sweden.

A. Lagerberg, B.S. Egardt, 2002, *Evaluation of Control Strategies for Automotive Powertrains with Backlash*, International Symposium on Advanced Vehicle Control, Hiroshima, Japan.

A. Lagerberg, B.S. Egardt, 2003, *Estimation of Backlash with Application to Automotive Powertrains*, IEEE Conference on Decision and Control, Hawaii, U.S.A.

A. Lagerberg, B.S. Egardt, 2004, *Estimation of Backlash in Automotive Powertrains – An Experimental Validation*, IFAC Symposium on Advances in Automotive Control, Salerno, Italy.

J. Maree, 2005, *Shaft Dynamics*, Research and Development Report, Stellenbosch Automotive Engineering, Atlantis, South Africa.

J.J. Momberg, 2005, *Unpublished Masters Thesis*, Department of Mechanical Engineering, University of Stellenbosch, Stellenbosch, South Africa.

J. Persson, 2004, *Integrated Powertrain Control – A Literature Survey on Longitudinal Vibrations, Driveability Aspects and Future Challenges*, Masters Thesis EX024/2003, Department of Signals and Systems, Chalmers University of Technology, Göteborg, Sweden.

M. Pettersson, 1996, *Driveline Modeling and Principles for Speed Control and Gear-Shift Control*, Thesis No. 564, Department of Electrical Engineering, Linköping University, S-581 83 Linköping, Sweden.

J. Treurnicht, 2005, *Personal discussion*, Department of Electrical and Electronic Engineering, University of Stellenbosch, Stellenbosch, South Africa.

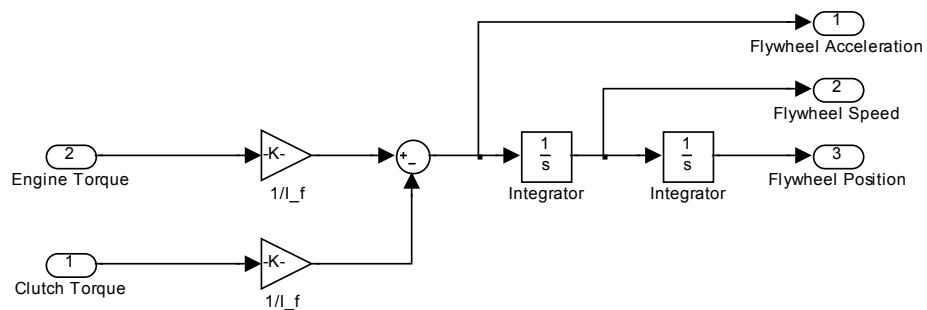
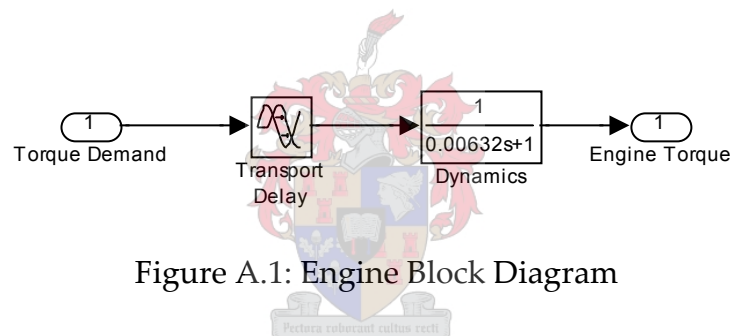
F.M. White, 1999, *Fluid Mechanics*, 4<sup>th</sup> Edition, WCB / McGraw Hill, Singapore.

J.Y. Wong, 2001, *Theory of Ground Vehicles*, 3<sup>rd</sup> Edition, John Wiley & Sons, New York, U.S.A.

# Drivetrain Model

# A

This appendix provides detailed Simulink block diagrams of each of these individual components. Figure 3.2.4 is an overview of the whole drivetrain model showing how the individual drivetrain components are interlinked.



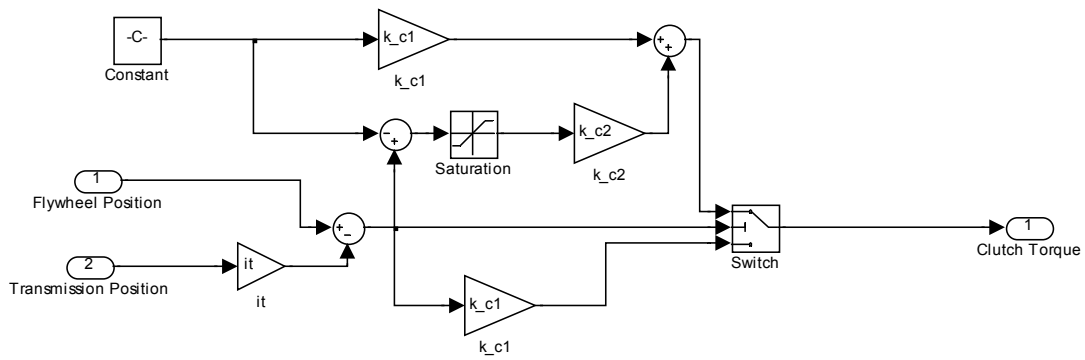


Figure A.3: Clutch Block Diagram

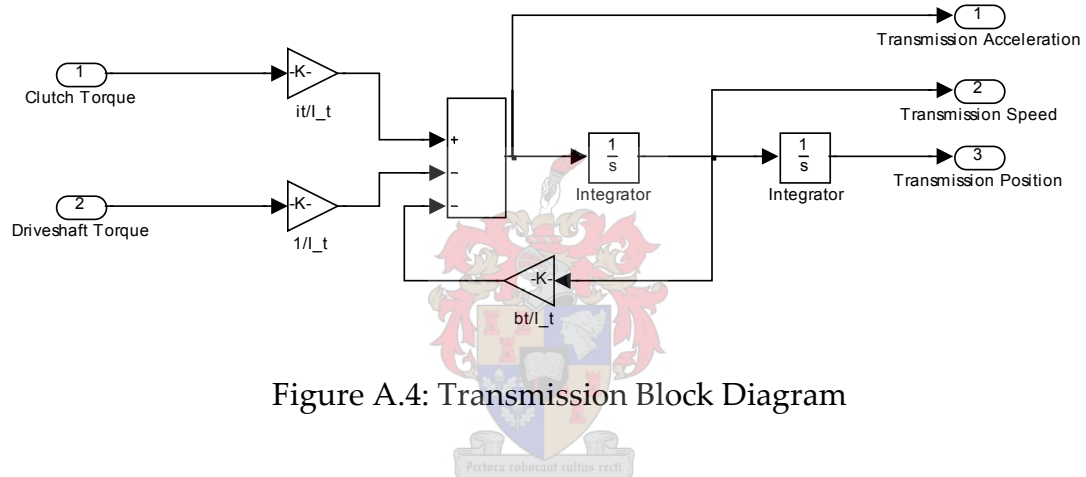


Figure A.4: Transmission Block Diagram

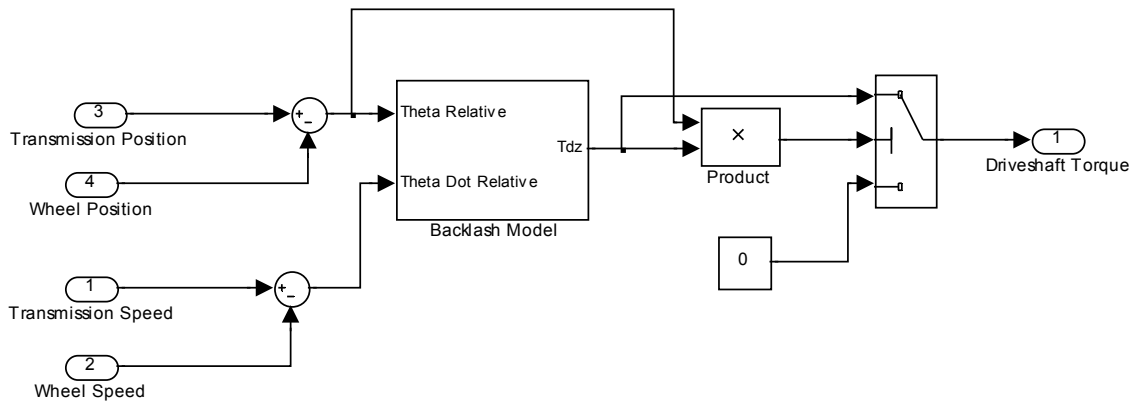


Figure A.5: Driveshaft Block Diagram

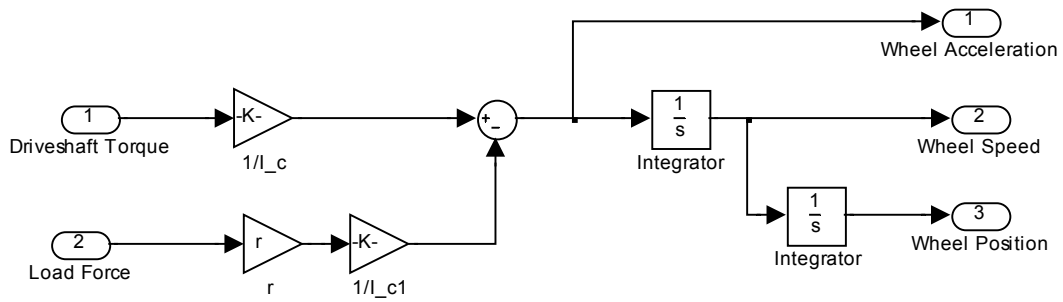


Figure A.6: Wheel Block Diagram

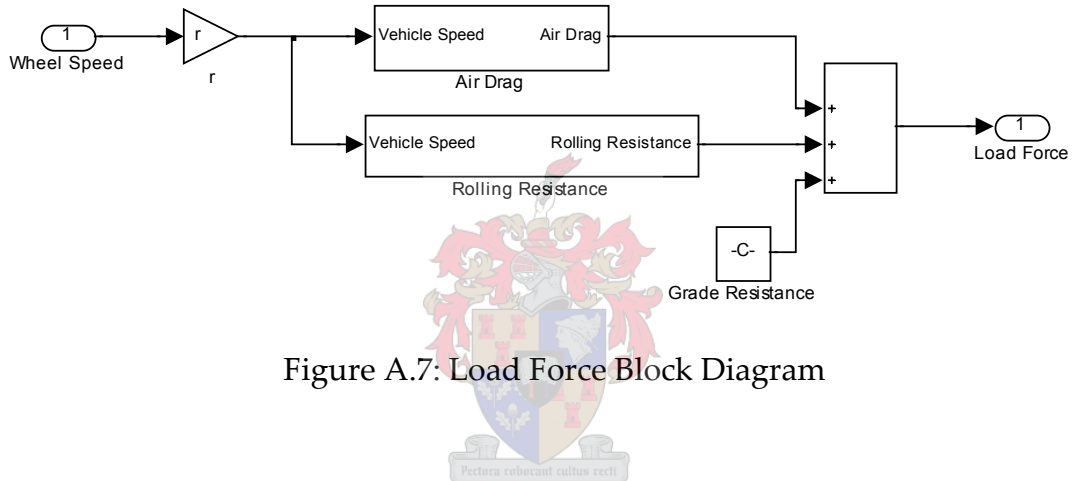


Figure A.7: Load Force Block Diagram

# Test-Rig

---

# B

This appendix provides more detailed photographs of the test-rig that was designed and manufactured for the experimental work completed in this thesis. The experiments were performed in an engine test cell. Figures B.1 and B.2 show the front and rear views of the fully assembled test-rig.



Figure B.1: Assembled Test-Rig (Front)

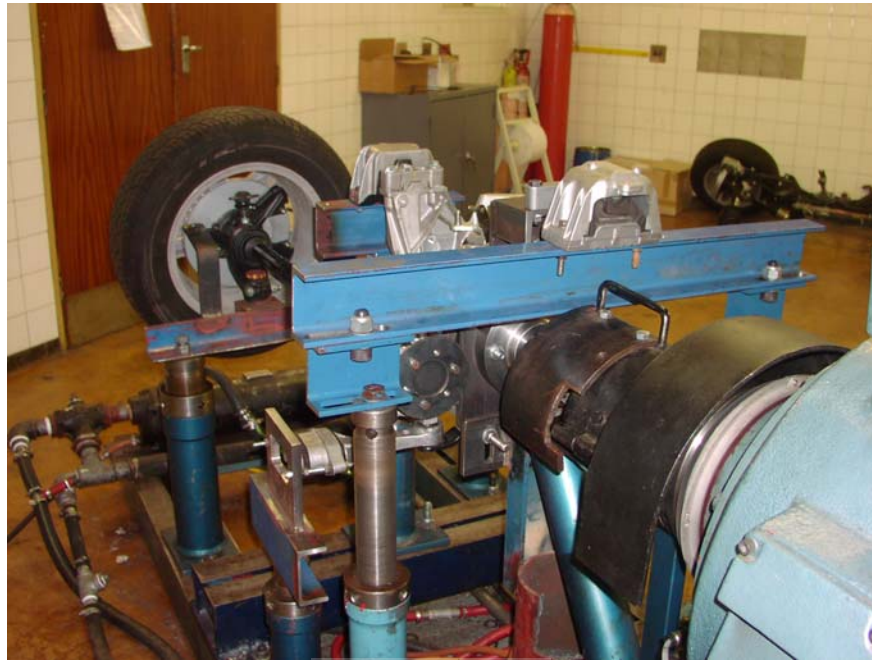


Figure B.2: Assembled Test-Rig (Rear)

Figure B.3 is a picture of the DC motor that was used to drive the drivetrain.



Figure B.3: DC Motor

Figure B.4 (shaft) and Figure B.5 (coupling) show how the DC motor and flywheel were connected.

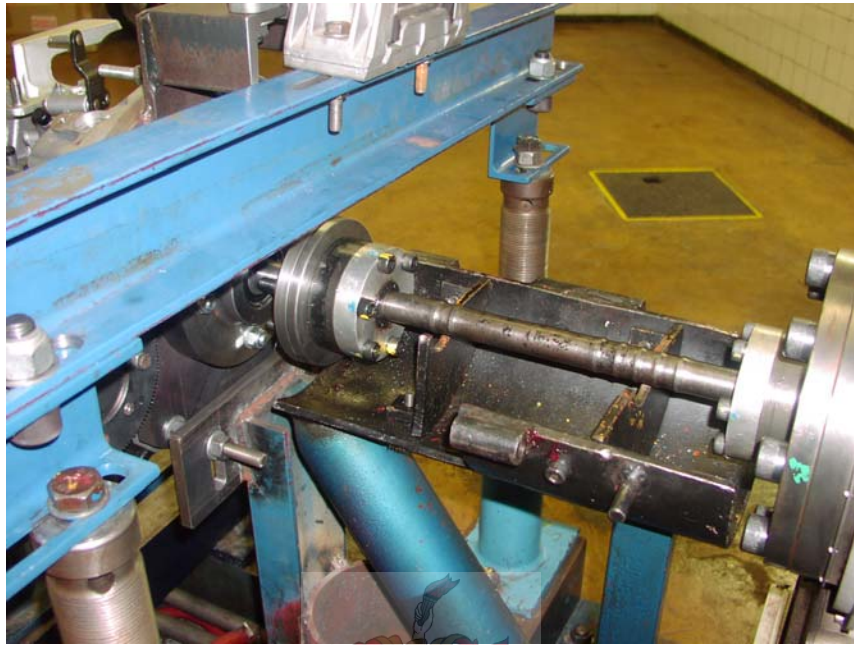


Figure B.4: Connecting Shaft

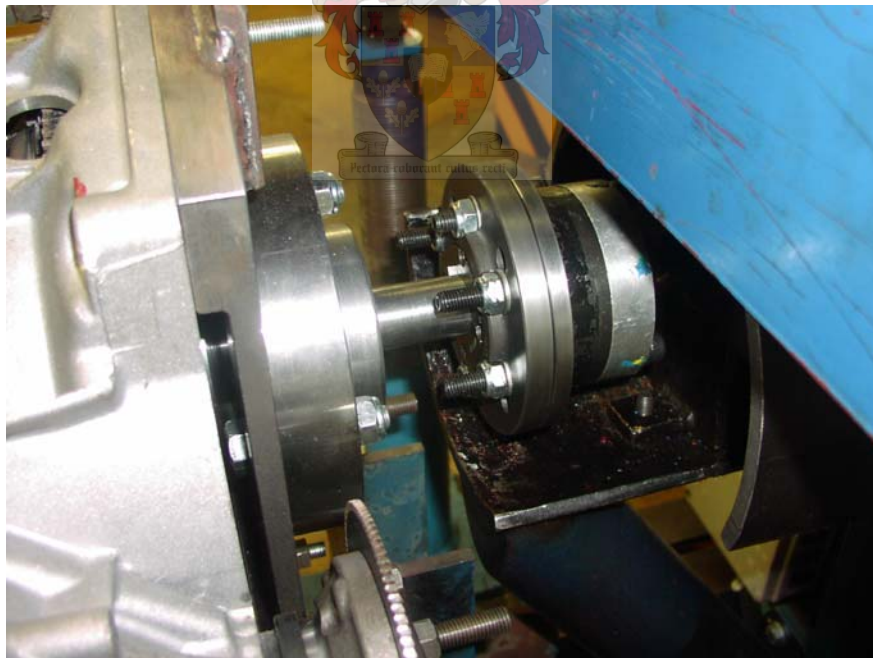


Figure B.5: Shaft Coupling



# Drivetrain Parameters

# C

Table C.1 provides a summary of the drivetrain parameters used in the vehicle simulations.

Table C.1: Drivetrain Parameters

Flywheel inertia	$I_f$	0.17 kg.m <sup>2</sup>
Clutch stiffness coefficient (0 – 0.2094 rad)	$k_{c1}$	854 N.m.rad <sup>-1</sup>
Clutch stiffness coefficient (0.2094 – 0.2443 rad)	$k_{c2}$	1672 N.m.rad <sup>-1</sup>
Transmission inertia	$I_t$	0.01 kg.m <sup>2</sup>
Transmission friction coefficient	$b_t$	0.01 N.m.s.rad <sup>-1</sup>
Overall gear ratio (1 <sup>st</sup> Gear)	$i_t$	12.98
Overall gear ratio (2 <sup>nd</sup> Gear)	$i_t$	7.65
Overall gear ratio (3 <sup>rd</sup> Gear)	$i_t$	5.16
Overall gear ratio (4 <sup>th</sup> Gear)	$i_t$	4.06
Overall gear ratio (5 <sup>th</sup> Gear)	$i_t$	3.30
Driveshaft stiffness coefficient	$k_s$	6420 N.m.rad <sup>-1</sup>
Drivetrain damping coefficient	$c_s$	90 N.m.s
Backlash angle	$2\alpha$	0.0785 rad
Wheel inertia	$I_w$	1.00 kg.m <sup>2</sup>
Wheel radius	$r_w$	0.32 m
Vehicle mass	$m$	1400 kg
Rolling resistant coefficient (speed independent)	$c_{r1}$	0.0136
Rolling resistant coefficient (speed dependent)	$c_{r2}$	$5.18 \times 10^7$
Vehicle coefficient of drag	$c_w$	0.3
Car frontal area	$A$	2.2 m <sup>2</sup>
Road Gradient	$\beta$	0 rad
Gravitational acceleration	$g$	9.81 m.s <sup>-2</sup>

# Discrete Estimator

# D

This appendix provides more detail on the discrete estimator used in the control system. Equations (D.1) and (D.2) are the basic discrete estimator equations.

$$\hat{x}(k) = \bar{x}(k) + L \cdot (y(k) - \bar{y}(k)) \quad (\text{D.1})$$

$$\bar{x}(k+1) = \Phi \cdot \hat{x}(k) + \Gamma \cdot u(k) \quad (\text{D.2})$$

The state-space system matrices of the estimator (A, B) were discretized ( $\Phi$ ,  $\Gamma$ ) for a sample time of 0.01 seconds. The calculations were performed using the 'c2d' function in Matlab. The resulting matrices are shown below:

$$\Phi = \begin{bmatrix} 0.9922 & -0.0097 & 0.0007 \\ 0.2551 & 0.9900 & 0.0008 \\ -16.805 & 0.6568 & 0.9494 \end{bmatrix} \quad (\text{D.3})$$

$$\Gamma = \begin{bmatrix} 0.0000 & 0.0001 \\ 0.0000 & -0.0001 \\ 0.0574 & -0.0000 \end{bmatrix} \quad (\text{D.4})$$